Predicting the efficacy of BH3 mimetics through the profiling of multiple protein complexes

Changju Chun[1,*], Ja Min Byun[2,*], Minkwon Cha[1,4,*], Hongwon Lee[3], Byungsan Choi[3], Hyunwoo Kim[3], Saem Hong[3], Yunseo Lee[3], Hayoung Park[3], Youngil Koh[2], and Tae-Young Yoon[1,3]

[1]School of Biological Sciences and Institute for Molecular Biology and Genetics, Seoul National University, Seoul 08826, South Korea

[2]Department of Internal Medicine, Seoul National University College of Medicine, Seoul National University Hospital, Seoul, South Korea

[3]Department of Biomarker Discovery, PROTEINA Co., Ltd, Seoul, South Korea

[4]Present address: Department of Physics, Pohang University of Science and Technology (POSTECH), Pohang, South Korea

*These authors equally contributed to this work.

Correspondence should be addressed to go01@snu.ac.kr or tyyoon@snu.ac.kr.

Abstract

BH3 mimetics are protein-protein interaction (PPI) inhibitors that saturate anti-apoptotic proteins in the BCL2 family to lift the resistance of cancer cells to apoptosis, a prominent example of protein complex-targeting therapies[1-4]. Despite the remarkable success of the BH3 mimetic ABT-199 in treating hematological malignancies[5-7], only a fraction of patients respond to ABT-199[8-10] and eventually develop resistance[11,12], necessitating the usage of predictive biomarkers for both initial responses and resistance development. We here used the single-molecule pull-down[13,14] and co-immunoprecipitation (co-IP)[15,16] platform to quantify more than 20 different types of PPI complexes using ~1.2×10^6 cells in total, revealing the latest rewired status of the BCL2-family PPI network. By comparing the obtained multi-dimensional data with BH3 mimetic efficacies determined *ex vivo*, we constructed an analysis model for ABT-199 efficacy. Our model designates the BCL2-BAX and BCLxL-BAK complexes to contrasting roles, with the former complex driving ABT-199 efficacy and the latter contributing to resistance development. We then applied this model to assist in therapeutic decision-making for acute myeloid leukemia patients in a prospective manner. Our work demonstrates a capability for the extensive characterization of PPI complexes in clinical specimens, potentially opening up a new avenue of precision medicine for protein complex-targeting therapies.

Cells utilize large protein-protein complexes in making complex decisions while reflecting various cellular states[17], with prominent examples including regulation of mechanistic target of rapamycin (mTOR) complexes in metabolism[18], inflammasomes in innate immunity[19] and BCL2 family complexes in apoptotic cell death[20]. Despite the unexpected breadth of associated proteins and their rapid turnover in these complexes, connectivity amongst several core components still defines a critical setpoint in cellular decision making. For example, across possible combinations of the BCL2 family proteins, the association between BAX and BAK forms proteinaceous pores that lead to mitochondria outer membrane permeabilization (MOMP), defining a point of no return for apoptosis initiation[21-23]. The survival and apoptotic pressure accrued in cells are reflected by the expression of anti- and pro-apoptotic proteins, tipping a balance in cellular decision toward life and death, respectively. While BCL2, BCLxL, and MCL1 make up the group of anti-apoptotic proteins that sequester BAX/BAK to prevent pore formation[20,24-26], pro-apoptotic proteins (such as BIM, BAD, and BID) share an alpha-helical BH3-domain and interact with either anti-apoptotic proteins or BAX/BAK[27-29], thereby unleashing the activation of BAX/BAK for pore formation[30,31].

In diseased states, cellular decisions are often misguided by chronic or spurious formation of these protein-protein complexes, as exemplified by mTOR complexes found in various cancers or type 2 diabetes[32,33] and inflammasomes in irritable bowel syndrome or neurodegenerative diseases[34,35]. Likewise, in many cancers, PPIs of the anti-apoptotic proteins are upregulated to suppress the activity of BAX/BAK, subsequently averting apoptosis initiation[25,31,36-38]. Massive effort has thus been made toward the development of PPI inhibitors that can disintegrate these disease-causing protein-protein complexes[39]. In particular, small-molecule drugs that structurally emulate the BH3 domain, collectively referred to as BH3

57 mimetics[1,2], have been arguably the most notable example in these endeavors. While sparing pro-
58 apoptotic proteins, BH3 mimetics are expected to bind selectively to the binding grooves of the
59 anti-apoptotic proteins to shut down their interactions with pro-apoptotic proteins and
60 BAX/BAK[3]. By introducing an azaindole moiety to ABT-263 (Navitoclax) that binds to both
61 BCL2 and BCLxL[40], ABT-199 (Venetoclax) has been developed to specifically bind to BCL2
62 with a sub-nM affinity[5]. ABT-199 was approved for the treatment of chronic lymphoid leukemia
63 (CLL) in 2016[41] and acute myeloid leukemia (AML) in 2018[9,42], which stimulated the
64 development of other BH3 mimetics that target other anti-apoptotic proteins beyond BCL2[3,43].

65 As evidenced in other targeted therapies, a precision medicine platform will enable the
66 tailored use of PPI inhibitors utilizing the unique molecular information of individual patients[44].
67 Indeed, despite the remarkable success of ABT-199 in treating CLL[6,7], more than 30% of AML
68 patients still fail to respond to ABT-199[8-10], and even many of the patients with initial favorable
69 responses eventually develop resistance to ABT-199[11,12]. These realities indicate unmet needs
70 where the patients may benefit from various treatment options if their initial responses and/or
71 resistance development can be predicted with high confidence. There exist, however, multiple
72 layers in the regulation of PPIs, such as post-translational modifications, protein conformational
73 changes, and cellular localizations, all of which would limit the direct translation of genomic and
74 proteomic information into an accurate prediction of the strengths of PPIs[20,45,46]. Indeed, genomic
75 and proteomic profiling have found limited uses in this technical niche. Genomic mutations, such
76 as G101V and D103E, have been found in the *BCL2* gene in relapsed CLLs, but these mutations
77 account for only a small fraction of ABT-199 resistance in AMLs[47-49]. Total expression levels of
78 BCL2 and other anti-apoptotic proteins are allegedly associated with the responses to
79 corresponding BH3 mimetics[50,51]. The resulting correlations are, however, not high enough to

80 warrant application of these protein levels as a predictive biomarker in clinical settings[50-53]. BH3
81 profiling is a functional approach that directly measures MOMP of cancer cell-derived
82 mitochondria induced by various BH3 peptides[54-56]. Despite its potential usefulness as a
83 prediction medicine platform for BH3 mimetics, the BH3 profiling method is not routinely used
84 in clinical settings presumably because of the technical difficulties involved with the derivation
85 and maintenance of cancer-derived mitochondria.

86 In this work, we hypothesized that the responsiveness of individual cancers to a PPI
87 inhibitor would be determined by the ever-evolving protein compositions of the target protein
88 complexes. In the case of BH3 mimetics, the heterocomplexes formed between the anti- and the
89 pro-apoptotic proteins and their detailed balances would be primarily responsible for mediating
90 the efficacy of BH3 mimetics in given cancers. A predictive algorithm may be trained when it is
91 possible to extensively profile BCL2-family protein complexes for as many cancers with known
92 responses as possible. To develop this capability for the profiling of protein-protein complexes
93 with minimal sample consumption and increased throughput, we adopted the single-molecule
94 pull-down and co-immunoprecipitation (co-IP) platform that directly immobilized target protein
95 complexes on the imaging plane of a single-molecule fluorescence microscope and counted the
96 number of protein complexes[13,14,16,57]. With the resulting sensitivity and accuracy of the assays,
97 we determined the populations of 20 different types of protein-protein complexes (and protein
98 levels) using only ~30,000 cells per each complex type, revealing the latest rewiring status of the
99 BCL2 family network in individual clinical samples.

100 We found that upon the introduction of bacterial toxin and BH3 mimetics, the
101 composition of the BCL2 protein-protein complexes showed dramatic changes while involving

102 only minor alterations in the corresponding protein levels, attesting to the importance of direct
103 profiling of PPI complexes. By comparing these multi-dimensional data with the efficacies of
104 BH3 mimetics determined *ex vivo*, we were able to train analysis models that revealed the
105 protein and PPI parameters that played the most prominent roles in mediating the BH3-mimetic
106 efficacies. In the case of ABT-199, the counts of two PPI complexes, BCL2-BAX and BCLxL-
107 BAK, were found to be the critical analysis parameters of contrasting roles, with the former
108 driving ABT-199 efficacy and the latter contributing to resistance development. In a similar
109 procedure, we also constructed an efficacy model for an MCL1-targeting inhibitor. Finally, we
110 applied the developed analysis model to therapeutic decisions for AML patients in a prospective
111 manner and confirmed the predictive power of the analysis model. Our work demonstrates the
112 use of single-molecule pull-down and co-IP in extensive profiling of PPI complexes with
113 accuracy that warrants clinical applications, suggesting a path toward precision medicine for the
114 protein complex-targeting therapies.

115

116 # Results

117 **Profiling BCL2-family protein complexes using single-molecule pull-down and co-IP**

118 To assess BCL2-family protein complexes and understand how apoptosis is suppressed in
119 individual cancers, we employed the single-molecule pull-down and co-IP platform to
120 characterize the PPI network among BCL2 family proteins[13-16]. We induced surface pull-down of
121 either one of the primary anti-apoptotic proteins (i.e., BCL2, BCLxL, or MCL1) from crude
122 extracts of cells onto the surface of the reaction chamber (Fig. 1a and Extended Data Fig. 1a-c).

After removal of the extract, we sequentially added a monoclonal antibody that binds to an interaction partner located on the surface-immobilized bait followed by a fluorescently labeled secondary antibody, which comprises of an immunoassay that detected a specific species of PPI complexes (Fig. 1b, left). Alternatively, by using a detection antibody that binds to an epitope directly on the surface bait, we could determine the total amount of surface-immobilized baits (Fig. 1b, right and Extended Data Fig. 1d-f).

To improve sensitivity and reproducibility in this protein complex detection method, we first optimized the lysis protocol[15,58]. Using HEK293T cells that co-expressed BCL2 and the BH3 domain of BIM (BIM_{BH3}), we found that mild lysis with cholesterol-like detergents, such as glycol-diosgenin (GDN) and digitonin, minimized dissociation of the model BCL2-BIM complexes (Extended Data Fig. 2). In addition, we confirmed that this lysis protocol did not induce the formation of spurious complexes even in dense cell extracts (i.e., at a total protein concentration of 5 to 10 mg/ml), indicating that all detected PPI complexes were formed in cellular environments (Fig. 1c). The BCL2 family proteins are known to undergo complex conformational changes during their activation[31,59]. Using the effector BAX protein as a precedent, we found that the detergent condition was critical in conserving the conformational states of BAX[60]. While Triton X-100 – often used in conventional co-IP methods – induced spurious conformational changes[61], the use of GDN or digitonin essentially preserved BAX's active conformations induced by the addition of a bacterial toxin, staurosporine (STS)[62] (Fig. 1d).

To minimize non-specific adsorption to the surface, we placed a high-density polyethylene glycol (PEG) layer between the IP antibodies and the glass coverslip[15,58] (Fig. 1a). This PEG layer proved to be essential in permitting direct surface IP of the target protein

145 complexes from the crude extracts, as well as in reducing background signals to a minimal level
146 on our single-molecule fluorescence imaging (Fig. 1e). Finally, to determine the assay signal, we
147 directly counted the number of single-molecule fluorescence spots (Extended Data Fig. 3a).
148 Compared with conventional approaches that integrate total fluorescence signals over a field of
149 view, this single-molecule counting method showed an enhanced sensitivity particularly when
150 there were ~2,000 or fewer individual PPI complexes per imaging area (Fig. 1f and Extended
151 Data Fig. 3b,c).

152 By combining the three technological factors of optimized lysis protocol, anti-fouling
153 PEG layer, and direct single-molecule counting, we were able to obtain statistically significant
154 counts for endogenous BCL2-BIM or BCL2-BAX complexes (CPXs) each using only ~30,000
155 AML cells (Fig. 1g,h). Using a non-small cell lung cancer cell line (PC9 cells), we confirmed a
156 similar capability where we detected 8 different BCLxL- and MCL1-protein complexes using
157 less than 50,000 PC9 cells each (Fig. 1i and Extended Data Fig. 4). In addition, three
158 independent inter-chip measurements yielded coefficients of variation (CVs) of less than 15% for
159 all assays and cell numbers tested, attesting to the high stability of the single-molecule co-IP
160 platform (Fig. 1i and Extended Data Fig. 4).

161

162 **Tracking the responses to apoptotic stress using single-molecule pull-down and co-IP**

163 To see whether the developed platform could track changes incurred in the BCL2-family PPI
164 network, we treated HL60 cells with 2 μM of STS and obtained extracts of these cells at different
165 time points across the treatment. Using flow cytometry, we found that the early apoptosis
166 population marked by high Annexin V staining began to surge at 1 hour of STS treatment at the

167 expense of the healthy cell population (Extended Data Fig. 5a,b). The late apoptosis population
168 stained with both Annexin V and PI rose after 4 hours. Necrosis populations were negative
169 throughout the flow cytometry study, indicating that the cells underwent apoptosis, not necrosis.

170 We found that the counts of active BAX and BAK increased dramatically as apoptosis
171 progressed (Fig. 2a). The BAX-BAK heterocomplex count, a more direct surrogate marker of
172 MOMP[63,64], started to rise concurrently with the active BAX and BAK counts, but continued to
173 grow through the late apoptosis stage. We next determined the total levels of anti-apoptotic
174 proteins (Fig. 2b). Through meticulous calibration of the immunolabeling efficiencies, we were
175 able to directly compare the amounts of the main anti-apoptotic proteins and found that the
176 BCL2 proteins were present in greater amounts in magnitudes of 4 to 5 compared to BCLxL and
177 MCL1, consistent with the known single dependence of HL60 on BCL2 (Fig. 2b and Extended
178 Data Fig. 6a,b). As apoptosis proceeded, the total levels of BCLxL and MCL1 gradually
179 decreased while the amount of BCL2 proteins showed a slight, yet significant increase (Fig. 2b).

180 In contrast to the marginal change in the BCL2 protein level, the heterocomplexes
181 forming between BCL2 and pro-apoptotic proteins showed dynamic changes throughout the
182 stages of apoptosis. We found that the BCL2 PPI complexes outnumbered those involving
183 BCLxL and MCL1, reconfirming the BCL2-dependence of HL60 cells (Fig. 2c,d). Remarkably,
184 the two protein-protein complexes showed contrasting behaviors. While the BCL2-BIM complex
185 counts gradually declined over time, the BCL2-BAX complex counts showed an upsurge with
186 the onset of the early apoptosis stage (Fig. 2c,d). Collectively, our comprehensive profiling of the
187 BCL2-family protein complexes revealed that to absorb the STS-induced apoptotic pressure in
188 HL60, the BCL2 proteins mainly worked to sequester the active BAX proteins while losing some

189 of the previously held BIM proteins. Presumably, under the STS treatment condition used, the
190 rate at which active BAXs were produced excelled the rate that BCL2 sequestered BAX proteins,
191 resulting in HL60 cells finally succumbing to apoptotic stress and initiating MOMP (Fig. 2a,d).

192

193 **Assessment of potential PPIs using protein interactor probes**

194 Our observations reassure the fact that the BCL2 family proteins – like many cell signaling
195 proteins – work by binding (or sequestering) to interaction partners[20]. In the case of elevated
196 survival pressure in HL60 cells provoked by STS treatment, the BCL2 proteins continuously
197 formed additional BCL2-BAX complexes to absorb apoptotic pressure (Fig. 2d). These data
198 prompted us to devise other types of assays that measure the capacity of the BCL2 family
199 proteins for making further protein-protein complexes beyond current complex populations.

200 To assess the strengths of potential PPIs, we used the same surface pull-down scheme to
201 immobilize anti-apoptotic BCL2 family proteins, which had been confirmed to induce minimal
202 IP crosstalk and non-specific adsorption (Fig. 2e). We then added various pro-apoptotic BCL2
203 proteins – tagged with enhanced green fluorescent proteins (eGFPs) – to the reaction chamber.
204 We reasoned that these PPI probes would bind to a pool of anti-apoptotic proteins that were
205 unoccupied, yet still be capable of making potential protein complexes (Fig. 2e). Indeed, This
206 PPI probe assay recapitulated many of the known biochemical features, such as a higher affinity
207 of BCL2 for BAD than for BIM and negligible interactions for BCL2-NOXA and MCL1-BAD
208 pairs[20] (Extended Data Fig. 7a). We also confirmed that these PPI probes did not induce
209 dissociation of the preformed, endogenous PPI complexes (Extended Data Fig. 7b).

210 With this probe binding assay (PBA), we examined the BCL2 proteins derived from the

211 STS-treated HL60 cells (Extended Data Fig. 5b). When we added the BH3 domain of BIM
212 (BIM_{BH3}-eGFP) as a PPI probe, BCL2 showed a significantly higher PBA count compared to
213 BCLxL and MCL1 (Fig. 2f). Considering the higher affinities of the BIM_{BH3} domain toward
214 BCLxL and MCL1 than toward BCL2, this high PBA count obtained for BCL2 implies that
215 BCL2 accounts for a dominant portion in sequestering pro-apoptotic proteins in HL60 (Fig. 2f
216 and Extended Data Fig. 7c). Remarkably, as the apoptosis stage proceeded, the PBA count of
217 BIM_{BH3} gradually reduced, despite the increase in the total BCL2 level, likely reflecting the
218 depletion of available BCL2 proteins with the formation of the BCL2-BAX complexes (Fig. 2c-
219 f). In addition, we examined the composition of the BCL2 protein-protein complexes in four
220 AML cell lines (Fig. 2g). When immobilizing the same number of total BCL2 proteins per field
221 of view, we found that the NB4 and U937 cells contained many more BCL2-BIM and BCL2-
222 BAX complexes – the two main species of BCL2 PPI complexes – than HL60 did (Fig. 2g,h).
223 This observation was accompanied by the PBA count being more than halved for NB4 and U937
224 compared to HL60 (Fig. 2i), which presumably reflected higher occupancies of BCL2 and thus
225 smaller pools of BCL2 proteins for potential PPIs in these cells (Fig. 2j).

226 Finally, we examined whether different PPI probes measure a same pool of BCL2
227 proteins or distinct BCL2 pools (i.e., each pool can be accessed by only dedicated PPI probes).
228 To answer this question, we added different PPI probes together and found that these added
229 probes directly competed with one another (Fig. 2k,l). In addition, the ratios of the PBA counts
230 for different cell lines were maintained across different PPI probes, indicating an existence of
231 one common BCL2 protein pool, rather than multiple, fragmented pools of BCL2 proteins
232 (compare Fig. 2i with Extended Data Fig. 7d-f).

233

234 **Tracing changes in the BCL2 family protein complexes evoked by BH3 mimetics**

235 Using the two types of assays established above (i.e., single-molecule immunoassay and PBA),
236 we sought to examine how BH3 mimetics induced apoptotic pressure in AMLs. We first treated
237 the HL60 cells with 100 nM ABT-199 for 24 hours and found that the BCL2 total level was
238 slightly increased by ~30% while the BCLxL and MCL1 levels were kept at minimal levels (Fig.
239 3a). In contrast, the amounts of active BAX and BAK as well as BAX-BAK heterocomplexes
240 steeply increased five-fold in response to the ABT-199 treatment, indicating active apoptosis
241 induction in HL60 (Fig. 3b). While the total populations of BAX and BAK were largely
242 maintained (Fig. 3c), most of the BCL2-BIM and BCL2-BAX complexes were dissociated after
243 24 hours due to ABT-199 (Fig. 3d). These data indicated that BAX released from BCL2 mainly
244 contributed to the steep increases in active BAX and BAK populations. In addition, the freeing
245 up of many BCL2 proteins by ABT-199 led to an increase in the PBA count, an observation in
246 direct opposite to the STS-treated case where the PBA count decreased over treatment time (Fig.
247 3e).

248 We wanted to track the dynamics of BCL2-BIM and BCL-BAX complexes in more detail,
249 particularly at the early time points of ABT-199 treatment. We treated HL60 at a higher
250 concentration of 300 nM ABT-199 and carried out PPI profiling at each hour point past initial
251 treatment (Extended Data Fig. 5c). Remarkably, the BCL2-BAX complex started to disintegrate
252 immediately upon ABT-199 treatment whereas the number of BCL2-BIM complexes remained
253 largely constant (Fig. 3f). The kinetics of BCL2-BAX dissociation coincided with the induction
254 of active BAX/BAK conformations and BAX-BAK heterocomplexes (Fig. 3g). These data

255 indicated that the dissociation of BCL2-BAX complexes by itself – without requiring BCL2-
256 BIM dissociation and additional BAX expression – was likely enough to evoke pro-apoptotic
257 pressure to initiate apoptosis (Fig. 3f-i)[47,65-67].

258 We examined whether the same complex dynamics also occurred in MCL1 inhibitor-
259 responding cells. In response to AZD-5591[68], U937 cells showed increased populations of the
260 active BAX and BAK proteins as well as the BAX-BAK heterocomplex, consistent with U937's
261 responsiveness to the MCL1 inhibitor (Fig. 3j). As in the case of ABT-199-treated HL60 cells,
262 the AZD-5591 treatment induced conspicuous dissociation of MCL1 PPI complexes (MCL1-
263 BIM and MCL1-BAK) confirmed by the dramatic increase in binding of the BIM_{BH3} probe for
264 MCL1 (Fig. 3k,l). However, unlike the case of HL60 where the other anti-apoptotic proteins
265 showed minimal changes, the BCLxL proteins in the U937 cells showed marked surges in their
266 protein complex counts, with the BCLxL-BAK complexes becoming the most dominant species
267 (Fig. 3m). Through detailed calibration of labeling efficiencies, we were able to find that the
268 observed increase in BCLxL-BAK far outnumbered the decrease in the MCL1-BAK complexes
269 (Fig. 3n and Extended Data Fig. 6a,c). We thus hypothesized that the majority of new BCLxL-
270 BAK complexes were formed by the sequestering of nascent BAK proteins, rather than through
271 being captured by those released from MCL1 (Fig. 3o). In summary, these data assured the
272 feasibility of the comprehensive profiling of BCL2-family protein complexes, which helped us
273 understand how apoptotic pressure was generated and then coped by the BCL2-family protein
274 network in individual cancers.

275

276

277 **Constructing an analysis model for ABT-199 efficacy with multi-dimensional PPI profiling**

278 So far, our data collectively suggest that the BH3 mimetics engage either protein complex
279 disintegration or saturation of anti-apoptotic proteins (or both) in the exertion of their efficacy. In
280 addition, our preliminary data suggest that a single-agent response can be expected when the
281 cancer cells have developed a singular dependence on a particular anti-apoptotic protein with
282 minimal compensation from other anti-apoptotic proteins (Extended Data Fig. 8). We thus
283 examined whether the multi-parameter data were used to train an analysis model that could
284 delineate the dependency on anti-apoptotic proteins for given cancers and predict their
285 responsiveness to BH3 mimetic drugs.

286 To this end, we analyzed 32 cases of primary AML samples. In this cohort, 30 cases were
287 collected from bone marrow mononuclear cells (BMMCs) and the other 2 cases were collected
288 from peripheral blood mononuclear cells (PBMCs), with clinical diagnosis composed of *de novo*
289 AML (n=17), relapsed AML (n=4), and secondary AML (n=11) (Supplementary Table 1). We
290 measured the *ex vivo* drug efficacy of ABT-199 and determined a normalized area under response
291 curve (AUC) for each sample (Fig. 4a, upper). We simultaneously performed single-molecule
292 PPI profiling on the same cohort samples in a blind manner. Of note, by virtue of the low sample
293 consumption and high data accuracy, we determined 22 different protein/PPI metrics for each
294 sample that consisted of ~1.2×10^6 cells in total (Fig. 4a, lower and Supplementary Table 2).

295 When comparing the correlation values of these protein/PPI assay data with AUC, the
296 three BCL2-related assay data – BCL2-BAD PBA, BCL2-BIM_{BH3} PBA, and BCL2-BAX CPX –
297 showed the highest correlations with *ex vivo* efficacy (Fig. 4b and Extended Data Fig. 9a-c). The
298 BCLxL- and MCL1-related metrics also showed appreciable, but lower correlation values,

299 indicating that most of the AML examined depended on BCL2 for their survival (Fig. 4b). Also,
300 it was notable that the BCL2-BIM complex showed a much lower correlation than the BCL2-
301 BAX complex count, echoing our observation that dissociation of the BCL2-BAX complexes
302 mainly mediated pro-apoptotic effects of ABT-199 in HL60 cells (Fig. 4c,d). The combination
303 between the three BCL2-related metrics, which showed the highest correlation to AUC,
304 improved the correlation to only a limited extent, indicating these three metrics reflected the
305 BCL2 dependence of the samples in a redundant manner (Extended Data Fig. 9d,e). We found
306 that addition of the BCLxL-BAK complex (with a negative coefficient) to the linear regression
307 model slightly but significantly improved the correlation to the AUC values (Fig. 4e).

308 We examined whether the generated model could reflect the changes in the BCL2 PPI
309 network as AML underwent clonal cancer evolution. For example, BC-7064, a case of primary
310 AML, showed favorable initial responses to a combined treatment of ABT-199 and azacitidine,
311 but later showed relapse after the treatment was discontinued (Fig. 4f). We carried out PPI
312 profiling for the initial (BC-7064) and the relapsed (BC-7064-R) samples using our platform (Fig.
313 4g). The initial sample showed a parameter combination for a strong ABT-199 effectiveness
314 (estimated score of 0.78), consisting of upregulated BCL2-BIM PBA and BCL2-BAX CPX
315 counts and a low BCLxL-BAK CPX level (Fig. 4g,h). On the other hand, the two BCL2-related
316 metrics were more than halved for BC-7064-R, indicating a weakened driving force for the ABT-
317 199 efficacy. Although the resistance factor BCLxL-BAK complex was also decreased for BC-
318 7064-R, the diminished BCL2 dependence led to an estimated score of 0.36, providing an
319 account for the relapse of this specific blood cancer (Fig. 4g-i).

320

321 **Construction of an MCL1 inhibitor efficacy model**

322 Next, we examined whether it was possible to train an analysis model for an MCL1 inhibitor,
323 AZD-5991, following a similar process we established for ABT-199. To this end, we determined
324 the *ex vivo* efficacy of AZD-5591 for the same primary AML cohort (27 out of 32 total samples)
325 and compared the determined AUC values with the BCL2 family metrics determined in Figure 4
326 (Supplementary Table 2). The MCL1 total level and the PBA count correlated with the AZD-
327 5591 efficacy, albeit with reduced correlations (Fig. 5a-c). The BIM_{BH3} PBA assay for BCLxL
328 showed a negative correlation with AZD-5991 efficacy (Fig. 5d). When we plotted the BCLxL
329 PBA counts for responsive (*ex vivo* AUC > 0.6) and non-responsive samples with respect to
330 AZD-5591, the non-responsive group exhibited distinctly higher counts, reflecting upregulated
331 activities of the BCLxL proteins in this group (Fig. 5e). These data collectively suggest that the
332 BCLxL proteins played major compensatory roles as MCL1 proteins were saturated with the
333 inhibitor molecules. In addition, MCL1 protein complexes showed only limited correlations,
334 consistent with the hypothesis we drew in Figure 3 that AZD-5591 might work by preventing
335 further binding of pro-apoptotic proteins to MCL1 (i.e., a saturation of MCL1 proteins), rather
336 than by inducing dissociation of the preexistent MCL1 PPI complexes (Fig. 5a).

337 The combination of multiple parameters, MCL1 total level, BCLxL-BIM_{BH3} PBA, and
338 BCLxL-BAK CPX, led to a linear regression model showing an optimized correlation with the
339 *ex vivo* AZD-5591 efficacy (Fig. 5f). We noted that the resulting correlation was weaker than
340 what we were able to optimize for ABT-199 (Fig. 4e). Moreover, while multiple, BCL2-related
341 parameters already showed high correlations with the ABT-199 efficacy (an indicator of the
342 singular dependence on BCL2) (Fig. 4b and Extended Data Fig. 9a-d), the MCL1-related metrics

343 had to be combined to improve the correlation, indicating an intricate balance and dynamic
344 between MCL1 and BCLxL protein pools (Fig. 5f and Extended Data Fig. 9f). Altogether, our
345 multi-parameter PPI data not only generates an analysis model for the efficacy of BH3 mimetics,
346 but also enables us to discern the relative contribution of each assay data and the detailed
347 balances among the protein complexes, which may hint at potential modes of action of the drugs.

348

349 **Using the PPI analysis model as a predictive biomarker for ABT-199 efficacy**

350 Finally, we asked whether the BCL2 PPI profiling could guide therapeutic decisions in a
351 prospective manner. BCL2 PPI profiling was carried out for seven patients treated with ABT-199
352 via oral administration. Treatment outcomes were assessed per European LeukemiaNet (ELN)
353 recommendations, and sequential samples were acquired throughout the treatment journey[69] (Fig.
354 6a).

355 Two samples, BC-6524 and BC-7230, showed contrasting patterns in our PPI profiling,
356 parallel with the disparate responses of the original patients to the ABT-199 treatment (Fig. 6b-d).
357 In the combination analysis model developed in Figure 4e, BC-6524 exhibited significantly
358 higher levels of counts for the BCL2-BIM_{BH3} PBA and BCL2-BAX CPX assays than BC-7230
359 while the BCLxL-BAK complex counts were low for both patients (Fig. 6b). These parameter
360 combinations indicated that BC-6524 would respond to a BCL2-targeted inhibitor with a high
361 estimated score of 0.90 (Fig. 6c, red). On the contrary, BC-7230 was predicted as a non-
362 responder with an estimated score of 0.27 (Fig. 6c, grey). Remarkably, these diagnostic
363 predictions correlated well with the *in vivo* responses: For the BC-6524 patient, peripheral blast
364 counts started to diminish from day 2, and complete remission was confirmed per bone marrow

365 examination (Fig. 6d, red). On the other hand, patient BC-7230 did not response to ABT-199 as
366 indicated by increasing peripheral blasts from day 3 (Fig. 6d, grey).

367 For six cases, including BC-6524 and BC-7230 illustrated above, the BCL2 PPI profiling
368 showed an outstanding performance in predicting the clinical responses (Extended Data Fig. 10
369 and Supplementary Table 3). One exception was BC-7052, where the patient initially responded
370 to ABT-199 but the duration of response was short-lived, discordant with a relatively high
371 estimated score of 0.64 (Extended Data Fig. 10a-c). Interestingly, in *ex vivo* efficacy
372 determination, the sample showed a high AUC value exactly matching the prediction by the
373 analysis model, pointing to a limit of the current model that was trained based on *ex vivo* drug
374 efficacy. The inclusion of the factors unique to cancer evolution in *in vivo* environments may
375 improve the predictive power of the model. For example, the BCLxL PBA count, which is not
376 included in the current model, was distinctively high for BC-7052, suggesting a possibility that
377 BCLxL proteins, initially largely unoccupied, become upregulated in its activity as the ABT-199
378 treatment was continued (Extended Data Fig. 10b).

379 In addition to the BC-7064 case examined in Figure 4f, we performed longitudinal
380 tracking for another case of BC-7107 to gain insights into how AML evolved with ABT-199
381 treatment. The patient had relapsed refractory disease with previous exposure to another
382 chemotherapeutic agent (Quizartinib) (Fig. 6e). The initial PPI profiling data showed a strongly
383 biased dependence on BCL2 (estimated score of 0.93), and the patient showed complete
384 remission for a combined treatment of ABT-199 and LDAC (Low-dose cytarabine) (Fig. 6f-h).
385 Unfortunately, after 1 month of treatment, relapse was noted (Fig. 6h). Remarkably, the PPI
386 profiling carried out after the relapse yielded virtually background signals for all three anti-

387 apoptotic proteins examined, indicating a possibility that this cancer might have developed a new
388 pathway to evade apoptosis initiation (Fig. 6g).

389

390 Discussion

391 In this work where we attempted to provide a precision medicine platform for protein complex-
392 targeting therapies, we used the single-molecule pull-down and co-IP platform to extensively
393 profile BCL2-family protein complexes in given AMLs. To this end, we optimized extraction
394 protocols that could be applied to clinical samples, which proved to preserve most PPI
395 complexes as well as specific conformations of the BCL2 family proteins through lysis. The anti-
396 fouling polymer layer minimized crosstalk and non-specific adsorption during surface pull-down.
397 In addition, the direct single-molecule counting of target PPI complexes retained its sensitivity
398 when there were only hundreds of PPI complexes pulled-down per each imaging area of ~10^4
399 μm^2. Altogether, the combination of these technical features allowed us to examine more than 20
400 different PPI species for clinical samples that consisted of as little as ~1.2×10^6 cells, reaching the
401 sensitivity and accuracy levels that could be applied to clinical specimens.

402 Given that BH3 mimetics are PPI inhibitors, conventional genomic and proteomic
403 profiling would be inherently limited in tracking the rewiring in the PPI network and thus in the
404 prediction of its response to given BH3 mimetics as well[50-53,70,71]. We indeed found that by
405 reflecting the cellular stress states, the BCL2-family protein complex counts showed dramatic
406 changes by more than three- to five-fold while the corresponding protein levels were marginally
407 changed (within 30%). Furthermore, rather than one fixed pathway for these changes, we found
408 that the two BH3 mimetics examined, ABT-199 and AZD-5991, affected BCL2-family protein

409 complexes in disparate ways, presumably because of their different modes of action (see below).
410 Thus, the analysis of genomic mutations and proteomic levels – and not of the connectivity
411 between them – could fall short in understanding the true complexity of BCL2 family biology
412 underlying the efficacy of BH3 mimetics.

413 Currently, there are competing hypotheses as to how BH3 mimetics induce apoptotic
414 pressure in cancer cells[31,72,73]. The activated BAX and BAK proteins – which form the BAX-
415 BAK pores and mediate MOMP – can be either newly expressed by the cells or released from
416 anti-apoptotic proteins. In the former scenario, the BH3 mimetics saturate the target anti-
417 apoptotic proteins to prevent further sequestering of nascent BAX and BAK proteins. In the latter,
418 BH3 mimetics squeeze into the binding groove of the anti-apoptotic proteins to induce the
419 release of previously held pro-apoptotic proteins. Detailed analyses on the increases and
420 decreases of relevant PPI complexes and protein levels, and thus their detailed balances, revealed
421 that ABT-199 mainly worked by inducing the disintegration of the pre-existing BCL2 protein
422 complexes. On the contrary, the MCL1 inhibitor AZD-5591 likely exerted its efficacy by
423 quenching the binding of newly produced BAK proteins to MCL1. Furthermore, tracing the two
424 types of the BCL2 protein complexes over time revealed that the dissociation of BCL2-BAX –
425 but not that of BCL2-BIM – was closely associated with the onset of apoptosis in AML cells
426 evoked by ABT-199. Also, in our multi-parametric measurement and linear regression analysis,
427 the BCL2-BAX amount was by far more closely related to the ABT-199 *ex vivo* efficacy than
428 BCL2-BIM. Thus, we concluded that in the case of AML we studied, the dissociation of BCL2-
429 BAX complexes mainly drove the efficacy of ABT-199.

430 These data compelled us to hypothesize a particular group of driver protein-protein

431 complexes that powerfully and positively correlated with the efficacy of the BH3 mimetics. We
432 also found protein or PPI metrics associated with the drug efficacy with negative coefficients,
433 which we defined as resistance complexes. The resulting analysis models included both driver
434 and resistance complexes, reflecting the competing roles of different anti-apoptotic proteins in
435 achieving the BH3-mimetic efficacy. In the combined model for ABT-199 effectiveness, BCL2-
436 BIM PBA and BCL2-BAX CPX worked as the driver complexes, while BCLxL-BAK CPX
437 worked as the resistance complex. However, the coefficient for BCLxL-BAK CPX was much
438 smaller than those of BCL2-related parameters, consistent with the singular dependence of
439 AMLs on BCL2[74,75]. On the other hand, the analysis model for AZD-5591 efficacy, consisting of
440 MCL1 total level, BCLxL-BAK CPX, and BCLxL-BIM_{BH3} PBA, assigned larger coefficients to
441 two BCLxL-involved parameters than it did for the MCL1 total level, suggesting that MCL1 was
442 in direct competition with BCLxL in mediating the effectiveness of AZD-5591.

443 Our analysis model has an inherent limitation in that it was generated based on the drug
444 efficacy determined *ex vivo*. Also, because of the small patient cohort size used in the study, it
445 remains to be tested whether the model would stay valid for larger cohorts. Despite these caveats,
446 we applied the analysis model to stratify ABT-199 responders prospectively and found that in six
447 out of seven cases, the prediction of the model highly correlated with the clinical responses.
448 Moreover, longitudinal tracking allowed us to take note of how the PPI connectivity rewired
449 itself across the BCL2 family proteins, which led to resistance development and relapse of the
450 cancers.

451 In summary, our work suggests that the single-molecule pull-down and co-IP platform
452 enables the examination of multiple protein-protein complexes in clinical specimens with high

453 sensitivity and accuracy. While the emerging technologies of single protein sequencing would
454 mainly serve as a discovery platforms[76], the platform demonstrated here would be used to
455 examine dozens of PPI complexes in clinical specimens, which are boiled down to be most
456 directly relevant to drug efficacies, thereby facilitating therapeutic decisions which would be
457 virtually impossible to achieve with genomic and proteomic profiling. Given the rapid rise in
458 protein complex-targeting therapies, it will be interesting to see whether the methodologies
459 developed here could be applied to other disease-causing protein complexes and drugs beyond
460 the BCL2 family and BH3 mimetics.

Methods

Antibodies

Anti-rabbit immunoglobulin G (IgG) with biotin conjugation (111-065-144; Jackson ImmunoResearch) and anti-mouse immunoglobulin G (IgG) with biotin conjugation (715-066-151; Jackson ImmunoResearch) were used to immobilize the antibodies for protein immunoprecipitation. Anti-RFP antibody with biotin conjugation (ab34771; Abcam) and anti-GFP antibody with biotin conjugation (ab6658; Abcam) were used to immuno-precipitate mCherry- or eGFP-labeled proteins.

MCL1 (94296S; Cell Signaling Technology), BCLxL (2764S; Cell Signaling Technology), BCL2 (4223S; Cell Signaling Technology), BAX (5023S; Cell Signaling Technology), and BAK (ab238515; Abcam) antibodies were used to immunoprecipitate the corresponding proteins. MCL1 (sc-12756; Santa Cruz Biotechnology), BCLxL (NBP1-47665; Novus Biologicals), BCL2 (sc-7382; Santa Cruz Biotechnology), BAX (MABC1176M; Sigma Aldrich), BAK (sc-517390; Santa Cruz Biotechnology), BIM (sc-374358; Santa Cruz Biotechnology), BAD (sc-8044; Santa Cruz Biotechnology), NOXA (sc-56169; Santa Cruz Biotechnology) antibodies were used to detect the corresponding proteins for immunoassay. Anti-rabbit immunoglobulin G (IgG) with Cy3 conjugation (111-165-046; Jackson ImmunoResearch) and anti-mouse immunoglobulin G (IgG) with Cy3 conjugation (715-165-151; Jackson ImmunoResearch) were used to label the detection antibodies for immunoassay.

Drug reagents

Staurosporine (HY-15141; MedChemExpress), ABT-199 (HY-15531; MedChemExpress), and

483 AZD-5991 (C-1060; Chemgood) were treated to the blood cancer cell lines or primary AML
484 cells. The concentration of the drugs was diluted to 10 mM with DMSO and stored at -80 °C.
485
486 **Cell culture**
487 HL60, THP-1, U937, and Ramos cells were purchased from Korean Cell Line Bank. HEK293T
488 and SU-DHL8 cells were purchased from ATCC. NB4 cells were purchased from DSMZ. SF9
489 cells were provided by S. H. Roh (Seoul National University School of Biological Sciences,
490 South Korea). PC9 cells were provided by Y. Hayata (Kyushu University Faculty of Medicine,
491 Japan).
492 HEK293T cells were cultured in DMEM (D6429; Sigma Aldrich) supplemented with 10% (v/v)
493 FBS (26140-079; Gibco) and 100 μg/ml penicillin/streptomycin (15140-122; Gibco). HL60,
494 THP-1, NB4, U937, Ramos, SU-DHL8, and PC9 cells were cultured in RPMI1640 (R8758;
495 Sigma Aldrich) supplemented with 10 % (v/v) FBS and 100 μg/ml penicillin/streptomycin. For
496 THP-1, 0.05 mM of 2-mercaptoethanol (M3148; Sigma Aldrich) was added to culture media. All
497 cells were incubated in a humidified incubator at 37 °C, 5% CO_2.
498 SF9 cells were cultured in Sf-900 II SFM (10902088; Gibco) supplemented with 10% FBS
499 (26140-079; Gibco) and 100 μg/ml penicillin/streptomycin. SF9 cells were then incubated on a
500 plat-form shaker rotating at ~130 rpm in a humidified incubator at 27 °C, non-CO_2.
501 HEK293T and PC9 cells were rinsed with cold DPBS (D8537; Sigma Aldrich) before collection.
502 Cells were collected with a scraper (90020; SPL Life Sciences) in 1 ml of cold DPBS.
503 Suspension-type cells were collected with centrifugation at 500 g for 5 minutes at 4 °C and
504 rinsed with 1 ml of cold DPBS. The cell suspensions were centrifuged at 500 g for 5 minutes at
505 4 °C. The supernatants were discarded after centrifugation and the cell pellets were stored at -80 °C

506 by snap-freezing with liquid nitrogen.

507

508 **Primary AML samples**

509 The cryo-preserved bone marrow mononuclear cells (BMMC) and peripheral blood mononuclear
510 cells (PBMC) collected from AML patients treated at Seoul National University Hospital were
511 used. Samples were collected between January 2014 and December 2019. Acute promyelocytic
512 leukemias and biphenotypic leukemias were excluded. Mononuclear cells were isolated by ficoll
513 gradient centrifugation. All samples were frozen in liquid nitrogen before flow cytometry
514 analysis and single-molecule co-IP. Aforementioned cell line collection protocol was applied for
515 primary AML cell collection. Culturing method for flow cytometry assay is described on the
516 Drug treatment and drug efficacy measurement section. Detailed information of each sample is
517 described in Supplementary Table 1. This study was conducted according to the Declaration of
518 Helsinki and was approved by the institutional review board of Seoul National University
519 Hospital (IRB number: H-1910-176-107).

520

521 **Fluorescence-labeled protein constructions**

522 All BCL2 family proteins (*BCL2* (HG10195-M; SinoBiological), *BCLxL* (HG10455-M;
523 SinoBiological), *MCL1* (HG10240-M; SinoBiological), BIM_{EL} (HG13816-G; SinoBiological),
524 *BAD* (HG10020-M; SinoBiological), *BAX* (HG11619-M; SinoBiological), *BAK* (HG10450-M;
525 SinoBiological) and *NOXA* (HG16548-U; SinoBiological)) were isolated from their respective
526 human cDNA. All cDNAs were cloned into *pCMV* vectors with eGFP or mCherry sequence to
527 generate fluorescence-labeled proteins by Gibson assembly.
528 The resulting plasmids were introduced into HEK293T cells through transient transfection.

529 Plasmid DNA with the amount of 10 μg was mixed with 30 μg of linear polyethyleneimine (PEI)
530 (23966-100; Polysciences) in 1 ml of serum-free DMEM. The mixture was introduced into
531 ~$2x10^6$ of HEK293T cells in a 90 mm^2 cell culture plate.
532 cDNA of BIM_{BH3} (MRQAEPADMRPEIWIAQELRRIGDEFNAYYARR) was isolated from
533 BIM_{EL} cDNA and cloned into *pFastBac1* vector with eGFP to generate eGFP-labeled BIM_{BH3}
534 proteins by Gibson assembly. The resulting plasmid was introduced into SF9 cells through Bac-
535 to-Bac System transfection. Plasmid DNA with the amount of 1 μg was mixed with 8 μl of
536 Cellfectin II Reagent (10362100; Thermo Fisher Scientific) in 200 μl of Sf-900 II SFM. The
537 mixture was introduced into ~$2x10^6$ of SF9 cells in a 6-well cell culture plate.
538
539 **Cell lysis**
540 All collected cell pellets were resuspended with the lysis buffer (0.2% or 1% (v/v) detergent, 50
541 mM HEPES with pH 7.4, 150 mM NaCl, 10% (v/v) glycerol, 1 mM EDTA, 2% (v/v) protease
542 inhibitor cocktail (P8340; Sigma Aldrich), 2% (v/v) phosphatase inhibitor cocktail 2 (P5726;
543 Sigma Aldrich), and 2% (v/v) phosphatase inhibitor cocktail 3 (P0044; Sigma Aldrich). Triton-
544 X100 (X100; Sigma Aldrich), glyco-diosgenin (GDN) (GDN101; Anatrace), digitonin (D141;
545 Sigma Aldrich), Tween 20 (P2287; Sigma Aldrich), 3-[(3-Cholamidopropyl) dimethylammonio]-
546 1-propanesulfonate hydrate (CHAPS) (C3023; Sigma Aldrich), and sodium dodecyl sulfate (SDS)
547 (L3771; Sigma Aldrich)) were used for optimizing the lysis protocol. Triton-X100, GDN,
548 digitonin, Tween 20, and CHAPS were used in 1% (v/v), and SDS was used in 0.2% (v/v) in
549 lysis buffer.
550 HEK293T cells expressing PPI probes (BIM_{BH3}-eGFP, BIM_{EL}-eGFP, BAD-eGFP, and NOXA-
551 eGFP) and SF9 cells expressing BIM_{BH3}-eGFP probe were lysed with Triton-X100 lysis buffer

552 for PPI probe binding assay (PBA). HEK293T cells for fluorescently labeled BCL2 family
553 proteins expression, blood cancer cell lines, and primary AML cells were lysed with GDN lysis
554 buffer for immunoassay and PBA.
555 The cell pellets were lysed with proper lysis buffer for 30 minutes at 4 °C. After lysis, the cell
556 suspensions were centrifuged at 15,000 g for 10 minutes at 4 °C. The supernatants were isolated
557 after centrifugation. The total protein concentration for each supernatant was measured with a
558 DC protein assay kit (5000113, 5000114, 5000115; Bio-Rad) following the manufacturer's
559 instructions. The total concentration of the fluorescence proteins in each supernatant was
560 measured with a Sense microplate reader (425-301; HIDEX). To quantify the fluorescence
561 proteins, a laser wavelength of 485 nm was used for eGFP excitation and 544 nm was used for
562 mCherry excitation respectively. Serial dilution experiments using eGFP and mCherry were
563 performed to generate the calibration curves. The aforementioned calibration curves were used to
564 quantify the concentrations of fluorescently labeled proteins. The supernatants were then
565 aliquoted and stored at -80 °C followed by snap-freezing with liquid nitrogen.
566
567 **Drug treatment and drug efficacy measurement**
568 All blood cancer cells and primary AML cells were precultured in a non-treated 25T flask for 3
569 hours before drug treatment. All cells were seeded in 4.5 ml of culture media and cultured in a
570 humidified incubator at 37 °C, 5% CO_2. STS, ABT-199, and AZD-5991 were then treated to
571 cells at various concentrations. All drugs were initially diluted with DMSO to 1 mM. For
572 experiments, serial dilution was performed with non-serum RPMI1640 to reach the target
573 concentration.
574 To determine the efficacy of drugs in blood cancer cells and primary AML cells, an

575 AnnexinV/PI apoptosis assay was performed. All cells treated with drugs were stained with
576 FITC-AnnexinV (640906; Biolegend) and PI (421301; Biolegend). After drug treatment, $5x10^5$
577 of cells were rinsed with cold DPBS and collected by centrifugation with 500 g for 5 minutes at
578 4 °C. After the supernatants were discarded, the cell pellets were resuspended with 100 µl of cold
579 AnnexinV-binding buffer (422201; Biolegend). After resuspension, 10 µl of FITC-AnnexinV
580 solution and 5 µl of PI solution were added into the cell suspensions. The cell suspensions were
581 incubated for 15 minutes at room temperature avoiding exposure to light. After that, 400 µl of
582 cold AnnexinV-binding buffer was added to avoid overstaining.
583 The stained cells were analyzed with a flow cytometry (SH800S; Sony). The proportions of
584 $AnnexinV^-/PI^-$ cells from each sample were calculated and converted to viability (%). Based on
585 the measured viabilities, the drug efficacy curve was fitted using the *logistic* function inside the
586 analysis software (OriginPro 2022), and the area under curve (AUC) was measured from the
587 fitted curve.
588
589 **Single-molecule pull-down and co-IP analysis for BCL2 family proteins**
590 **Single-molecule pull-down for BCL2 family proteins**: 5 µg/ml of NeutrAvidin (31000;
591 Thermo Fisher Scientific) was loaded into each reaction chamber of the PROTEINA imaging
592 chip (PROTEINA) and incubated for 10 minutes. The imaging chip was washed with TritonX-
593 100-buffer (0.1% (v/v) TritonX-100, 50 mM HEPES with pH 7.4, 150 mM NaCl) to remove
594 unbound NeutrAvidin. Biotin-conjugated IgGs were loaded to each reaction chamber with 1:200
595 in TritonX-100-buffer and incubated for 10 minutes. The imaging chip was washed with
596 TritonX-100-buffer. Then, primary antibodies for target proteins were loaded into each reaction
597 chamber with 1:100 in TritonX-100 buffer and incubated for 10 minutes. The imaging chip was

598 washed with GDN-buffer (0.01% (w/v) GDN, 50 mM HEPES with pH 7.4, 150 mM NaCl, 1%
599 (v/v) Glycerol, 1 mM EDTA). After washing, crude cell extracts were diluted based on the total
600 protein concentrations and were loaded into each reaction chamber. When immunoprecipitating
601 fluorescence-labeled proteins, anti-RFP or anti-GFP antibodies were loaded with 1:200 in
602 TritonX-100-buffer and incubated for 20 minutes instead of the biotin-conjugated IgGs.
603
604 **Single-molecule co-IP for BCL2 family proteins**: To measure the total level of BCL2 family
605 proteins, 1 mg/ml of cell extracts were loaded into each reaction chamber and incubated for 1
606 hour. To measure the total level of BAX and BAK, the cell extracts were activated with Triton
607 X-100 before pull-down. After activation, the cell extracts were loaded into each reaction
608 chamber and incubated for 1 hour. The level of PPI complex was measured by loading 2 mg/ml
609 of cell extracts into each reaction chamber with a 2 hour incubation time. After pull-down, the
610 primary antibodies to detect matching proteins or protein complexes were loaded into each
611 reaction chamber with 1:100 in TritonX-100-buffer and incubated for 1 hour. Cy3-conjugated
612 IgGs with 1:1,000 in TritonX-100-buffer were loaded into each reaction chamber to label the
613 detection antibodies with 20 minutes incubation.
614 To measure the PBA, 1 mg/ml of cell extracts were loaded into each reaction chamber and
615 incubated for 1 hour. After that, the imaging chip was washed with GDN-buffer. The HEK293T
616 or SF9 cells expressing PPI probes were lysed with TritonX-100 lysis buffer. The crude cell
617 extracts were diluted and then incubated for 10 minutes on the immunoprecipitated bait proteins.
618
619 **Assessment of PPIs using single-molecule fluorescence imaging:** Single-molecule
620 fluorescence signal was assessed using the PI-View system (PROTEINA). The PI-View system

621 allows single-molecule fluorescence imaging for two different excitation lasers, 488 nm and 532
622 nm. By adapting an extremely sensitive scalable complementary metal-oxide semiconductor
623 (sCMOS) camera in the system, the emitted photons from a single fluorophore can be collected
624 efficiently with superior signal-to-noise ratio. An autofocus system installed in the PI-View
625 system provides high-quality image acquisition during whole imaging chip assessment. To detect
626 fluorescence signal, the imaging chip after performing all steps required for single-molecule co-
627 IP analysis was put on a chip holder placed on the top of the PI-View system. To quantify the
628 fluorescence signal of each chamber, ~10 different locations were imaged with 89 x 89 μm^2 size
629 of the field of view. Each image was acquired for 5 frames with 0.1 s time resolution, and those
630 frames were averaged to generate a single snapshot. This frame average process can reduce
631 random noise and improve signal-to-noise ratio. From a processed image, single-molecule
632 fluorescence spots and sum of pixel signals were quantified using software provided by
633 PROTEINA.
634
635 **Drug efficacy prediction model analysis**
636 Drug efficacy prediction models for AML patients were generated using linear regression
637 analysis by MATLAB 2021a. The PPI profiles from the primary AML cells were all converted to
638 a $\log_2$ scale. The number of single-molecule fluorescence spots fewer than 100 counts was fixed
639 to the minimum value (100 counts) for log transformation. For BCLxL-BAX, BCLxL-BAK, and
640 BCL2-BAK PPI complexes, the total fluorescence signal data were used instead of single-
641 molecule spot data, and the fluorescence signals less than 10^7 were fixed to the minimum value
642 (10^7, background level) for log transformation. The AUCs from the primary AML cells were
643 normalized by *normAUC= 1- (AUC/Maximal AUC)* and were used as *ex vivo* drug efficacy. The

644 correlation between the transformed PPI profiles and *ex vivo* drug efficacy was calculated
645 through linear regression. After that, the coefficients of the PPI metrics and the statistical
646 indicators (Pearson's R and *p*-value) of the model were collected from each regression model.
647 The models with low significance ($p > 0.05$), containing a low significant ($p > 0.05$) PPI metrics
648 as a variable, or inconsistent with common biological features, were excluded during analysis.
649 Custom MATLAB code for modeling is available upon request.
650

651 **Acknowledgements**

652 We thank Shi Ho Kim and Jason Sang Hyun Park for critical reading of the manuscript, and
653 Changwon Kim, Gee Sung Eun, and Tae Gyun Kim for active discussion concerning data
654 analysis. This work was supported by the National Grants for Leading Scientists (NRF-
655 2021R1A3B1071354 to T.-Y.Y.) and the Bio Medical Technology Development Program (NRF-
656 2018M3A9E2023523 to T.-Y.Y.) funded by the National Research Foundation of South Korea.
657 This work was also supported by the Korea Health Technology R&D Project of the Korea Health
658 Industry Development Institute (KHIDI) (HI14C1277 to Y.K.) funded by the Ministry of Health
659 & Welfare of South Korea.
660

661 **Author contributions**

662 T.-Y.Y. conceived of and supervised the project. C.C., J.M.B., M.C., H.L., B.C., Y.K., and T.-
663 Y.Y. designed the experiments. C.C. and M.C. performed the single-molecule pull-down and co-
664 IP experiments. C.C. and H.K. measured the inter-chip CVs of the immunoassays. J.M.B. and
665 Y.K. collected and characterized primary AML samples and performed *in vivo* ABT-199
666 treatment journey. C.C., Y.L., and H.P. developed the PPI probes for PBA. C.C., M.C., B.C.,

667 H.K., S.H., and Y.L. performed the PPI profiling for the primary AML samples. C.C. and M.C.
668 measured the *ex vivo* drug efficacies of the primary AML samples. H.L. developed the *ex vivo*
669 drug efficacy predicting programs. C.C. analyzed and visualized all data. C.C. and T.-Y.Y. wrote
670 the manuscript with inputs from all authors.
671

672 **Competing interests**

673 C.C., M.C., H.L., B.C., Y.L., S.H., Y.K., and T.-Y.Y. filed a patent on these findings (10-2020-
674 0157961).
675

676 ## References

677 1 Ashkenazi, A., Fairbrother, W. J., Leverson, J. D. & Souers, A. J. From basic apoptosis
678 discoveries to advanced selective BCL-2 family inhibitors. *Nat Rev Drug Discov* **16**, 273-
679 284, doi:10.1038/nrd.2016.253 (2017).

680 2 Cory, S., Roberts, A. W., Colman, P. M. & Adams, J. M. Targeting BCL-2-like Proteins to
681 Kill Cancer Cells. *Trends Cancer* **2**, 443-460, doi:10.1016/j.trecan.2016.07.001 (2016).

682 3 Billard, C. BH3 Mimetics: Status of the Field and New Developments. *Mol Cancer Ther*
683 **12**, 1691-1700, doi:10.1158/1535-7163.Mct-13-0058 (2013).

684 4 Czabotar, P. E., Lessene, G., Strasser, A. & Adams, J. M. Control of apoptosis by the
685 BCL-2 protein family: implications for physiology and therapy. *Nat Rev Mol Cell Bio* **15**,
686 49-63, doi:10.1038/nrm3722 (2014).

687 5 Souers, A. J. *et al.* ABT-199, a potent and selective BCL-2 inhibitor, achieves antitumor
688 activity while sparing platelets. *Nat Med* **19**, 202-208, doi:10.1038/nm.3048 (2013).

689 6 Seymour, J. F. *et al.* Bcl-2 Inhibitor ABT-199 (GDC-0199) Monotherapy Shows Anti-
690 Tumor Activity Including Complete Remissions In High-Risk Relapsed/Refractory (R/R)
691 Chronic Lymphocytic Leukemia (CLL) and Small Lymphocytic Lymphoma (SLL). *Blood*
692 **122** (2013).

693 7 Roberts, A. W. *et al.* Targeting BCL2 with Venetoclax in Relapsed Chronic Lymphocytic
694 Leukemia. *New Engl J Med* **374**, 311-322, doi:10.1056/NEJMoa1513257 (2016).

695 8 Konopleva, M. *et al.* Efficacy and Biological Correlates of Response in a Phase II Study
696 of Venetoclax Monotherapy in Patients with Acute Myelogenous Leukemia. *Cancer*
697 *Discov* **6**, 1106-1117, doi:10.1158/2159-8290.CD-16-0313 (2016).

698 9 DiNardo, C. D. *et al.* Venetoclax combined with decitabine or azacitidine in treatment-

699 naive, elderly patients with acute myeloid leukemia. *Blood* **133**, 7-17, doi:10.1182/blood-
700 2018-08-868752 (2019).
701 10 Pollyea, D. A. *et al.* Venetoclax in Combination with Hypomethylating Agents Induces
702 Rapid, Deep and Durable Responses in Patients with AML Ineligible for Intensive
703 Therapy. *Blood* **132**, doi:10.1182/blood-2018-99-117179 (2018).
704 11 Guieze, R. *et al.* Mitochondrial Reprogramming Underlies Resistance to BCL-2
705 Inhibition in Lymphoid Malignancies. *Cancer Cell* **36**, 369-384 e313,
706 doi:10.1016/j.ccell.2019.08.005 (2019).
707 12 Thijssen, R. *et al.* Resistance to ABT-199 induced by microenvironmental signals in
708 chronic lymphocytic leukemia can be counteracted by CD20 antibodies or kinase
709 inhibitors. *Haematologica* **100**, e302-306, doi:10.3324/haematol.2015.124560 (2015).
710 13 Ha, T. *et al.* Single-molecule fluorescence spectroscopy of enzyme conformational
711 dynamics and cleavage mechanism. *Proc Natl Acad Sci U S A* **96**, 893-898,
712 doi:10.1073/pnas.96.3.893 (1999).
713 14 Jain, A. *et al.* Probing cellular protein complexes using single-molecule pull-down.
714 *Nature* **473**, 484-U322, doi:10.1038/nature10016 (2011).
715 15 Lee, H. W. *et al.* Profiling of protein-protein interactions via single-molecule techniques
716 predicts the dependence of cancers on growth-factor receptors. *Nat Biomed Eng* **2**, 239-
717 253, doi:10.1038/s41551-018-0212-3 (2018).
718 16 Lee, H. W. *et al.* Real-time single-molecule co-immunoprecipitation analyses reveal
719 cancer-specific Ras signalling dynamics. *Nat Commun* **4**, 1505,
720 doi:10.1038/ncomms2507 (2013).
721 17 Alberts, B. The cell as a collection of protein machines: Preparing the next generation of

722 molecular biologists. *Cell* **92**, 291-294, doi:Doi 10.1016/S0092-8674(00)80922-8 (1998).
723 18 Saxton, R. A. & Sabatini, D. M. mTOR Signaling in Growth, Metabolism, and Disease
724 (vol 168, pg 960, 2017). *Cell* **169**, 362-362, doi:10.1016/j.cell.2017.03.035 (2017).
725 19 Broz, P. & Dixit, V. M. Inflammasomes: mechanism of assembly, regulation and
726 signalling. *Nat Rev Immunol* **16**, 407-420, doi:10.1038/nri.2016.58 (2016).
727 20 Kale, J., Osterlund, E. J. & Andrews, D. W. BCL-2 family proteins: changing partners in
728 the dance towards death. *Cell Death Differ* **25**, 65-80, doi:10.1038/cdd.2017.186 (2018).
729 21 Kalkavan, H. & Green, D. R. MOMP, cell suicide as a BCL-2 family business. *Cell*
730 *Death Differ* **25**, 46-55, doi:10.1038/cdd.2017.179 (2018).
731 22 Wei, M. C. *et al.* Proapoptotic BAX and BAK: a requisite gateway to mitochondrial
732 dysfunction and death. *Science* **292**, 727-730, doi:10.1126/science.1059108 (2001).
733 23 Chipuk, J. E., Bouchier-Hayes, L. & Green, D. R. Mitochondrial outer membrane
734 permeabilization during apoptosis: the innocent bystander scenario. *Cell Death Differ* **13**,
735 1396-1402, doi:10.1038/sj.cdd.4401963 (2006).
736 24 Moore, V. D. & Letai, A. BH3 profiling - Measuring integrated function of the
737 mitochondrial apoptotic pathway to predict cell fate decisions. *Cancer Lett* **332**, 202-205,
738 doi:10.1016/j.canlet.2011.12.021 (2013).
739 25 Ku, B., Liang, C. Y., Jung, J. U. & Oh, B. H. Evidence that inhibition of BAX activation
740 by BCL-2 involves its tight and preferential interaction with the BH3 domain of BAX.
741 *Cell Res* **21**, 627-641, doi:10.1038/cr.2010.149 (2011).
742 26 Willis, S. N. *et al.* Proapoptotic Bak is sequestered by Mcl-1 and Bcl-x(L), but not Bcl-2,
743 until displaced by BH3-only proteins. *Gene Dev* **19**, 1294-1305,
744 doi:10.1101/gad.1304105 (2005).

745 27 Sarosiek, K. A. *et al.* BID Preferentially Activates BAK while BIM Preferentially
746 Activates BAX, Affecting Chemotherapy Response. *Mol Cell* **51**, 751-765,
747 doi:10.1016/j.molcel.2013.08.048 (2013).
748 28 Robin, A. Y. *et al.* Crystal structure of Bax bound to the BH3 peptide of Bim identifies
749 important contacts for interaction. *Cell Death Dis* **6**, doi:ARTN e1809
750 10.1038/cddis.2015.141 (2015).
751 29 Ren, D. *et al.* BID, BIM, and PUMA are essential for activation of the BAX- and BAK-
752 dependent cell death program. *Science* **330**, 1390-1393, doi:10.1126/science.1190217
753 (2010).
754 30 Czabotar, P. E. *et al.* Bax Crystal Structures Reveal How BH3 Domains Activate Bax and
755 Nucleate Its Oligomerization to Induce Apoptosis. *Cell* **152**, 519-531,
756 doi:10.1016/j.cell.2012.12.031 (2013).
757 31 Westphal, D., Kluck, R. M. & Dewson, G. Building blocks of the apoptotic pore: how
758 Bax and Bak are activated and oligomerize during apoptosis. *Cell Death Differ* **21**, 196-
759 205, doi:10.1038/cdd.2013.139 (2014).
760 32 Zou, Z. L., Tao, T., Li, H. M. & Zhu, X. mTOR signaling pathway and mTOR inhibitors
761 in cancer: progress and challenges. *Cell Biosci* **10**, doi:10.1186/s13578-020-00396-1
762 (2020).
763 33 Laplante, M. & Sabatini, D. M. mTOR Signaling in Growth Control and Disease. *Cell*
764 **149**, 274-293, doi:10.1016/j.cell.2012.03.017 (2012).
765 34 Shen, H. H. *et al.* NLRP3: A promising therapeutic target for autoimmune diseases.
766 *Autoimmun Rev* **17**, 694-702, doi:10.1016/j.autrev.2018.01.020 (2018).
767 35 Heneka, M. T., McManus, R. M. & Latz, E. Inflammasome signalling in brain function

768 and neurodegenerative disease. *Nat Rev Neurosci* **19**, 610-621, doi:10.1038/s41583-018-
769 0055-7 (2018).
770 36 Um, H. D. Bcl-2 family proteins as regulators of cancer cell invasion and metastasis: a
771 review focusing on mitochondrial respiration and reactive oxygen species. *Oncotarget* **7**,
772 5193-5203, doi:DOI 10.18632/oncotarget.6405 (2016).
773 37 Kelly, P. N. & Strasser, A. The role of Bcl-2 and its pro-survival relatives in
774 tumourigenesis and cancer therapy. *Cell Death Differ* **18**, 1414-1424,
775 doi:10.1038/cdd.2011.17 (2011).
776 38 Hockings, C. *et al.* Mcl-1 and Bcl-x(L) sequestration of Bak confers differential
777 resistance to BH3-only proteins. *Cell Death Differ* **25**, 721-734, doi:10.1038/s41418-017-
778 0010-6 (2018).
779 39 Lu, H. Y. *et al.* Recent advances in the development of protein-protein interactions
780 modulators: mechanisms and clinical trials. *Signal Transduct Tar* **5**, doi:ARTN 213
781 10.1038/s41392-020-00315-3 (2020).
782 40 Tse, C. *et al.* ABT-263: A potent and orally bioavailable Bcl-2 family inhibitor. *Cancer*
783 *Res* **68**, 3421-3428, doi:10.1158/0008-5472.Can-07-5836 (2008).
784 41 Stilgenbauer, S. *et al.* Venetoclax in relapsed or refractory chronic lymphocytic leukaemia
785 with 17p deletion: a multicentre, open-label, phase 2 study. *Lancet Oncol* **17**, 768-778,
786 doi:10.1016/S1470-2045(16)30019-5 (2016).
787 42 Wei, A. H. *et al.* Venetoclax Combined With Low-Dose Cytarabine for Previously
788 Untreated Patients With Acute Myeloid Leukemia: Results From a Phase Ib/II Study. *J*
789 *Clin Oncol* **37**, 1277-1284, doi:10.1200/JCO.18.01600 (2019).
790 43 Townsend, P. A., Kozhevnikova, M. V., Cexus, O. N. F., Zamyatnin, A. A. & Soond, S. M.

791 BH3-mimetics: recent developments in cancer therapy. *J Exp Clin Canc Res* **40**,
792 doi:ARTN 355 10.1186/s13046-021-02157-5 (2021).

793 44 Jameson, J. L. & Longo, D. L. Precision Medicine - Personalized, Problematic, and
794 Promising. *New Engl J Med* **372**, 2229-2234, doi:10.1056/NEJMsb1503104 (2015).
795 45 Ruvolo, P. P., Deng, X. & May, W. S. Phosphorylation of Bcl2 and regulation of
796 apoptosis. *Leukemia* **15**, 515-522, doi:10.1038/sj.leu.2402090 (2001).
797 46 Yip, K. W. & Reed, J. C. Bcl-2 family proteins and cancer. *Oncogene* **27**, 6398-6406,
798 doi:10.1038/onc.2008.307 (2008).
799 47 Blombery, P. *et al.* Acquisition of the Recurrent Gly101Val Mutation in BCL2 Confers
800 Resistance to Venetoclax in Patients with Progressive Chronic Lymphocytic Leukemia.
801 *Cancer Discovery* **9**, 342-353, doi:10.1158/2159-8290.Cd-18-1119 (2019).
802 48 Blombery, P. *et al.* Multiple BCL2 mutations cooccurring with Gly101Val emerge in
803 chronic lymphocytic leukemia progression on venetoclax. *Blood* **135**, 773-+,
804 doi:10.1182/blood.2019004205 (2020).
805 49 Tausch, E. *et al.* Venetoclax resistance and acquired BCL2 mutations in chronic
806 lymphocytic leukemia. *Haematologica* **104**, doi:ARTN e434
807 10.3324/haematol.2019.222588 (2019).

808 50 Pan, R. *et al.* Selective BCL-2 inhibition by ABT-199 causes on-target cell death in acute
809 myeloid leukemia. *Cancer Discov* **4**, 362-375, doi:10.1158/2159-8290.CD-13-0609
810 (2014).
811 51 Punnoose, E. A. *et al.* Expression Profile of BCL-2, BCL-XL, and MCL-1 Predicts
812 Pharmacological Response to the BCL-2 Selective Antagonist Venetoclax in Multiple

813 Myeloma Models. *Mol Cancer Ther* **15**, 1132-1144, doi:10.1158/1535-7163.MCT-15-
814 0730 (2016).
815 52 Davids, M. S. *et al.* Phase I First-in-Human Study of Venetoclax in Patients With
816 Relapsed or Refractory Non-Hodgkin Lymphoma. *J Clin Oncol* **35**, 826-833,
817 doi:10.1200/JCO.2016.70.4320 (2017).
818 53 Song, T. *et al.* Bcl-2 phosphorylation confers resistance on chronic lymphocytic
819 leukaemia cells to the BH3 mimetics ABT-737, ABT-263 and ABT-199 by impeding
820 direct binding. *Brit J Pharmacol* **173**, 471-483, doi:10.1111/bph.13370 (2016).
821 54 Villalobos-Ortiz, M., Ryan, J., Mashaka, T. N., Opferman, J. T. & Letai, A. BH3 profiling
822 discriminates on-target small molecule BH3 mimetics from putative mimetics. *Cell*
823 *Death Differ* **27**, 999-1007, doi:10.1038/s41418-019-0391-9 (2020).
824 55 Ryan, J., Montero, J., Rocco, J. & Letai, A. iBH3: simple, fixable BH3 profiling to
825 determine apoptotic priming in primary tissue by flow cytometry. *Biol Chem* **397**, 671-
826 678, doi:10.1515/hsz-2016-0107 (2016).
827 56 Bhatt, S. *et al.* Reduced Mitochondrial Apoptotic Priming Drives Resistance to BH3
828 Mimetics in Acute Myeloid Leukemia. *Cancer Cell* **38**, 872-890 e876,
829 doi:10.1016/j.ccell.2020.10.010 (2020).
830 57 Lee, H. W. *et al.* Real-time single-molecule coimmunoprecipitation of weak protein-
831 protein interactions. *Nat Protoc* **8**, 2045-2060, doi:10.1038/nprot.2013.116 (2013).
832 58 Choi, B. *et al.* Single-molecule functional anatomy of endogenous HER2-HER3
833 heterodimers. *Elife* **9**, doi:ARTN e53934 10.7554/eLife.53934 (2020).
834 59 Dengler, M. A. *et al.* BAX Activation: Mutations Near Its Proposed Non-canonical BH3
835 Binding Site Reveal Allosteric Changes Controlling Mitochondrial Association. *Cell Rep*

836 **27**, 359-373 e356, doi:10.1016/j.celrep.2019.03.040 (2019).
837 60 Peyerl, F. W. *et al.* Elucidation of some Bax conformational changes through
838 crystallization of an antibody-peptide complex. *Cell Death Differ* **14**, 447-452,
839 doi:10.1038/sj.cdd.4402025 (2007).
840 61 Zhang, Z. *et al.* Bax forms an oligomer via separate, yet interdependent, surfaces. *J Biol*
841 *Chem* **285**, 17614-17627, doi:10.1074/jbc.M110.113456 (2010).
842 62 Antonsson, A. & Persson, J. L. Induction of apoptosis by staurosporine involves the
843 inhibition of expression of the major cell cycle proteins at the G(2)/m checkpoint
844 accompanied by alterations in Erk and Akt kinase activities. *Anticancer Res* **29**, 2893-
845 2898 (2009).
846 63 Srivastava, A. K. *et al.* BAX-BAK heterodimer as a pharmacodynamic biomarker of on-
847 target drug action of Mcl-1 inhibitors to evaluate in-vivo effectiveness. *J Clin Oncol* **36**,
848 doi:DOI 10.1200/JCO.2018.36.15_suppl.2582 (2018).
849 64 Zhou, L. Y. & Chang, D. C. Dynamics and structure of the Bax-Bak complex responsible
850 for releasing mitochondrial proteins during apoptosis. *J Cell Sci* **121**, 2186-2196,
851 doi:10.1242/jcs.024703 (2008).
852 65 Willis, S. N. *et al.* Apoptosis initiated when BH3 ligands engage multiple Bcl-2 homologs,
853 not Bax or Bak. *Science* **315**, 856-859, doi:10.1126/science.1133289 (2007).
854 66 Anderson, M. A. *et al.* The BCL2 selective inhibitor venetoclax induces rapid onset
855 apoptosis of CLL cells in patients via a TP53-independent mechanism. *Blood* **127**, 3215-
856 3224, doi:10.1182/blood-2016-01-688796 (2016).
857 67 Chen, H. C. *et al.* An interconnected hierarchical model of cell death regulation by the
858 BCL-2 family. *Nat Cell Biol* **17**, 1270-1281, doi:10.1038/ncb3236 (2015).

859 68 Tron, A. E. *et al.* Discovery of Mcl-1-specific inhibitor AZD5991 and preclinical activity
860 in multiple myeloma and acute myeloid leukemia. *Nat Commun* **9**, 5341,
861 doi:10.1038/s41467-018-07551-w (2018).
862 69 Dohner, H. *et al.* Diagnosis and management of AML in adults: 2017 ELN
863 recommendations from an international expert panel. *Blood* **129**, 424-447,
864 doi:10.1182/blood-2016-08-733196 (2017).
865 70 Roberts, A. W. *et al.* Efficacy of venetoclax in relapsed chronic lymphocytic leukemia is
866 influenced by disease and response variables. *Blood* **134**, 111-122,
867 doi:10.1182/blood.2018882555 (2019).
868 71 Mato, A. R. *et al.* Real-world outcomes and management strategies for venetoclax-treated
869 chronic lymphocytic leukemia patients in he United States. *Haematologica* **103**, 1511-
870 1517, doi:10.3324/haematol.2018.193615 (2018).
871 72 Liu, Z. *et al.* Direct Activation of Bax Protein for Cancer Therapy. *Med Res Rev* **36**, 313-
872 341, doi:10.1002/med.21379 (2016).
873 73 Walensky, L. D. Targeting BAX to drug death directly. *Nat Chem Biol* **15**, 657-665,
874 doi:10.1038/s41589-019-0306-6 (2019).
875 74 Bensi, L. *et al.* Bcl-2 oncoprotein expression in acute myeloid leukemia. *Haematologica*
876 **80**, 98-102 (1995).
877 75 Banker, D. E., Groudine, M., Norwood, T. & Appelbaum, F. R. Measurement of
878 spontaneous and therapeutic agent-induced apoptosis with BCL-2 protein expression in
879 acute myeloid leukemia. *Blood* **89**, 243-255 (1997).
880 76 Alfaro, J. A. *et al.* The emerging landscape of single-molecule protein sequencing
881 technologies. *Nat Methods* **18**, 604-617, doi:10.1038/s41592-021-01143-1 (2021).

882 # Figures and legends

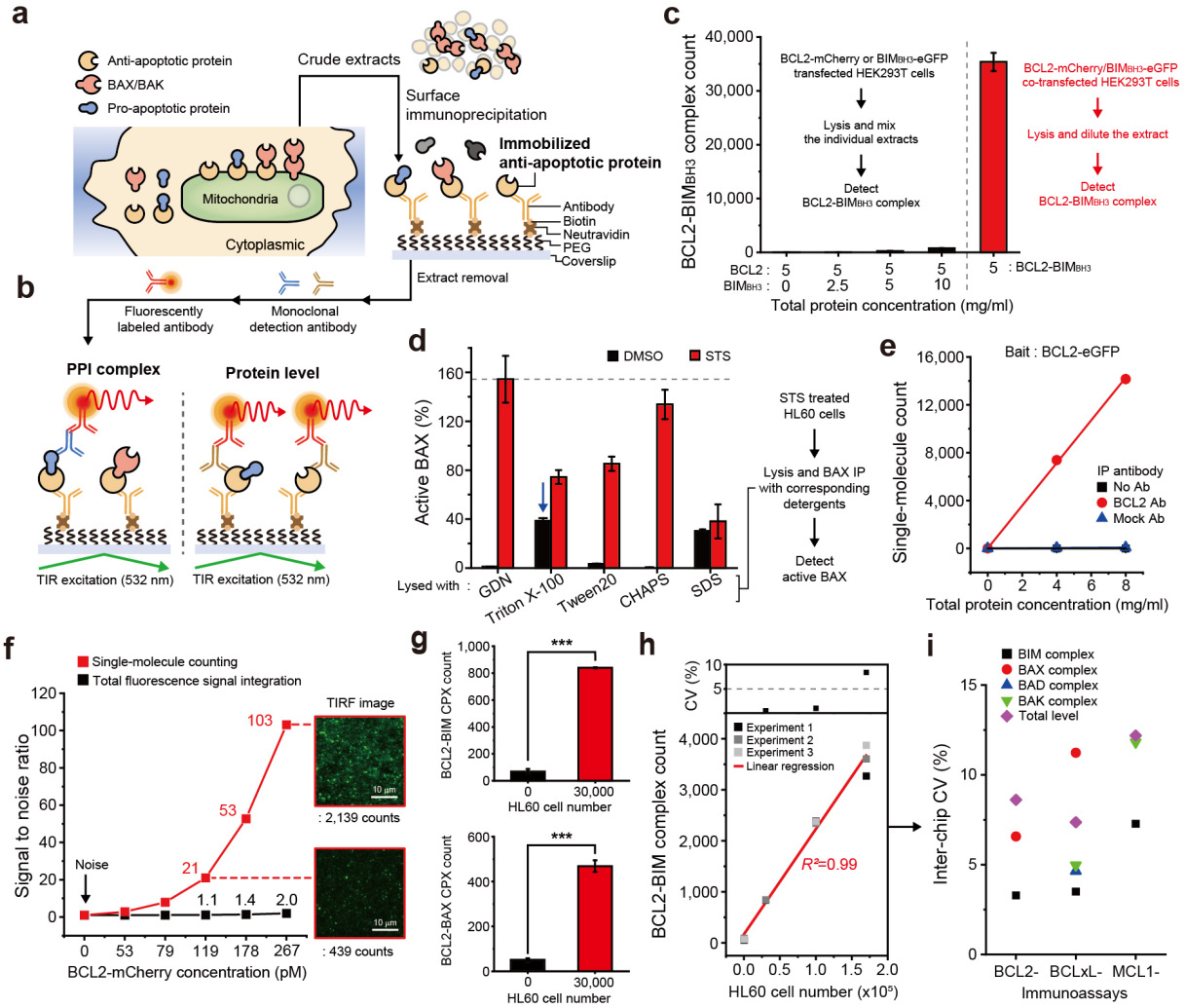

883

884 **Fig. 1: Profiling BCL2-family protein complexes using single-molecule co-IP. a,** Schematic
885 for the surface immunoprecipitation (IP) of BCL2 family proteins. Anti-apoptotic proteins
886 (BCL2, BCLxL, MCL1) in cell extracts were lysed with mild detergent and immobilized onto
887 the surface of the reaction chamber. **b,** Schematic of sandwich-type immunoassay selectively
888 detecting PPI complex (left) and the total level of surface bait (right). The fluorescence signals
889 from detection antibodies were imaged by a single-molecule co-IP platform. **c,** Comparing the
890 formation of BCL2-BIM_{BH3} PPI complex in an intracellular environment by BCL2-

891 mCherry/BIM_{BH3}-eGFP co-transfection (red) and *in vitro* mixing of two individual extracts
892 expressing BCL2-mCherry and BIM_{BH3}-eGFP (black). **d,** Relative changes of active BAX level
893 from the STS treated HL60 cells after lysed with different detergent types. The monoclonal
894 antibody 6A7 was used to detect the activated BAX[60]. Spurious BAX activation by Triton X-100
895 was indicated (blue). **e,** Surface-immobilization of the matching IP antibodies immunoprecipitate
896 BCL2-eGFP from the crude extract with high specificity. **f,** Comparison of signal to noise ratio
897 (SNR) from single molecule counting analysis (red) and total fluorescence signal integrating
898 analysis (black). The raw data to calculate the SNRs are described in Extended Data Fig. 2. **g,**
899 Counts of endogenous BCL2-related PPI complexes (BCL2-BIM, BCL2-BAX) from the 30,000
900 HL60 cells by using immunoassay. Error bars represent mean ± s.d. from independent inter-chip
901 measurement ($n \geq 2$). (Two-sided two-sample *t*-test, P=1.46x10^{-5}, 1.11x10^{-5} respectively). **h**,
902 Counts of endogenous BCL2-BIM PPI complexes and inter-chip CVs from the fixed numbers of
903 HL60 cells ($n \geq 2$). **i**, Inter-chip CVs obtained from independent inter-chip measurement for all
904 the immunoassays and cell numbers ($n \geq 2$).

905

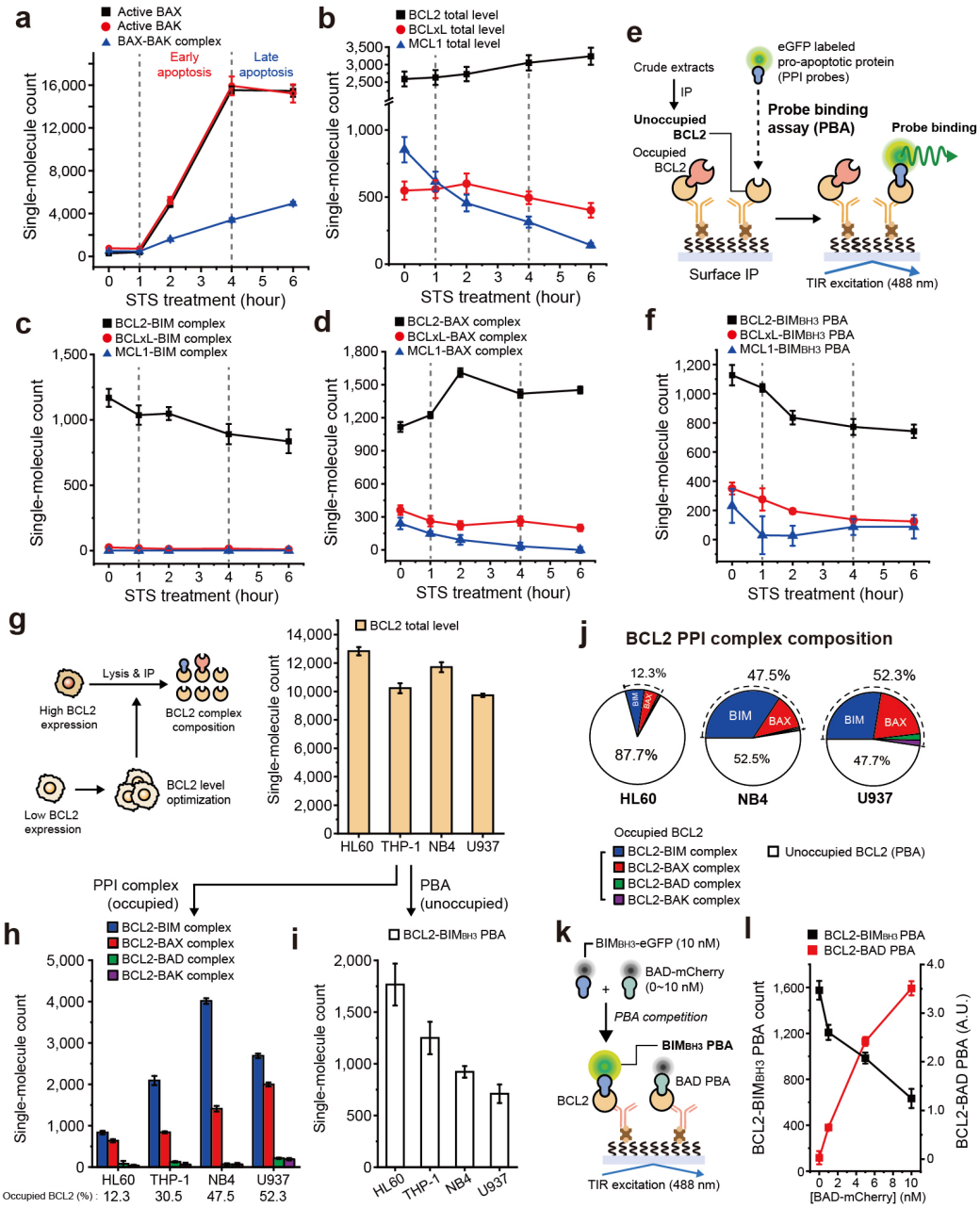

Fig. 2: Tracking the responses to intrinsic apoptotic stress with single-molecule co-IP. a-d, Changes of endogenous PPI profiles of HL60 cells through the apoptosis progression by 2 μM of STS. (a) Active BAX/BAK level, (b) Total levels of anti-apoptotic proteins (BCL2, BCLxL, MCL1), (c) BIM complexes with anti-apoptotic proteins, (d) BAX complexes with anti-apoptotic proteins. **e**, Schematic for the PPI probe binding assay (PBA) for measuring unoccupied

912 populations of surface-immobilized anti-apoptotic proteins. **f,** Changes of BIM_{BH3} PBAs for anti-
913 apoptotic proteins from HL60 cells through the apoptosis progression by STS. **g,** Schematic for
914 the comparison of the BCL2 PPI complex compositions in different AML cell lines. The density
915 of surface-immobilized BCL2 was constantly maintained by optimizing the total protein
916 concentration of crude cell extracts for all AML cell lines (HL60, THP-1, NB4, U937). **h,**
917 Compositions of the BCL2 complexes (BIM, BAX, BAD, BAK) in four different AML cell lines.
918 The labeling efficiencies of the immunoassays were applied. **i,** BCL2-BIM_{BH3} PBA counts of
919 four AML cell lines. **j,** The PPI complex compositions of BCL2 in HL60, NB4, and U937 cell
920 extracts. **k,** Schematic of binding competition between two PPI probes, BIM_{BH3}-eGFP and BAD-
921 mCherry, on surface immobilized BCL2 from HL60 cells. **l,** Changes of BCL2-BIM_{BH3} PBA and
922 BCL2-BAD PBA with increasing amounts of BAD probe. BIM_{BH3} PPI probe was presented in
923 10 nM.

924

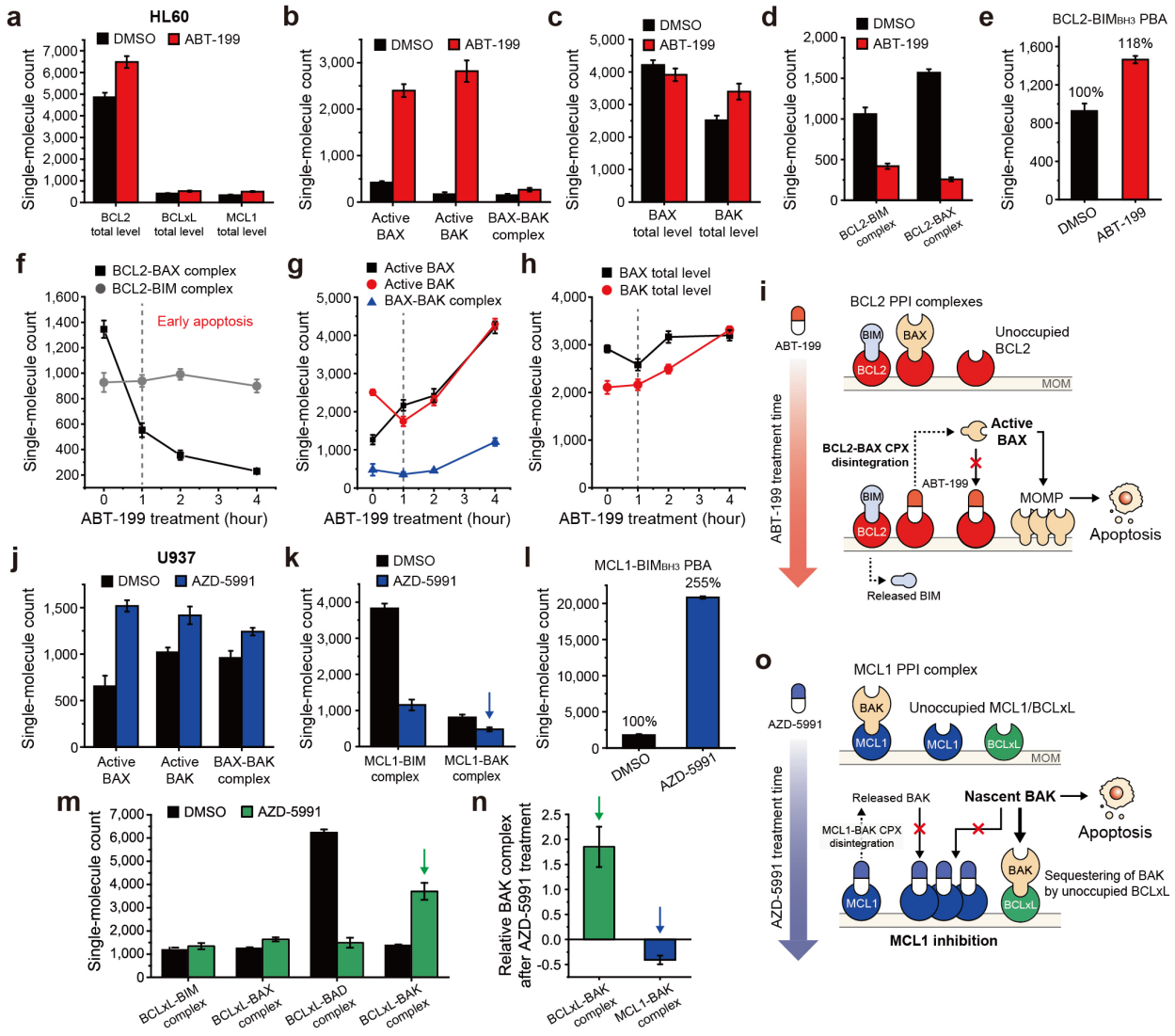

925

926 **Fig. 3: Changes in the BCL2 family PPI complexes evoked by BH3 mimetics. a-e,** Changes
927 of BCL2-related PPI profile in HL60 cells after ABT-199 (100 nM, 24 hours) treatment. (a) Total
928 levels of anti-apoptotic proteins, (b) Active BAX/BAK level, (c) Total levels of BAX/BAK, (d)
929 BCL2 complexes (BIM, BAX), (e) BCL2-BIM$_{BH3}$ PBA. **f-h,** Changes of PPI profile of HL60
930 cells after higher concentration of ABT-199 (300 nM) treatment. (f) BCL2 complexes (BIM,
931 BAX), (g) Active BAX/BAK level, (h) Total levels of BAX/BAK. **i,** Schematic model of mode
932 of action of ABT-199. **j-l**, Changes of MCL1-related PPI profile of U937 cells after AZD-5991

933 (100 nM, 24 hours) treatment. (j) Active BAX/BAK level, (k) MCL1 complexes (BIM, BAK), (l)
934 MCL1-BIM_{BH3} PBA. The decrease of MCL1-BAK complex after AZD-5991 treatment was
935 indicated (blue). **m,** Changes of BCLxL complexes (BIM, BAX, BAD, BAK) from U937 cells
936 after AZD-5991 (100 nM, 24 hours) treatment. The increase of BCLxL-BAK complex after
937 AZD-5991 treatment was indicated (green). **n,** Comparison of relative changes of BAK
938 complexes from U937 cells after AZD-5991 treatment. The relative changes were obtained from
939 the indicated data in (k) and (m). **o,** Schematic model of mode of action of AZD-5991. (d, k, m)
940 The labeling efficiencies of the immunoassays were applied.

941

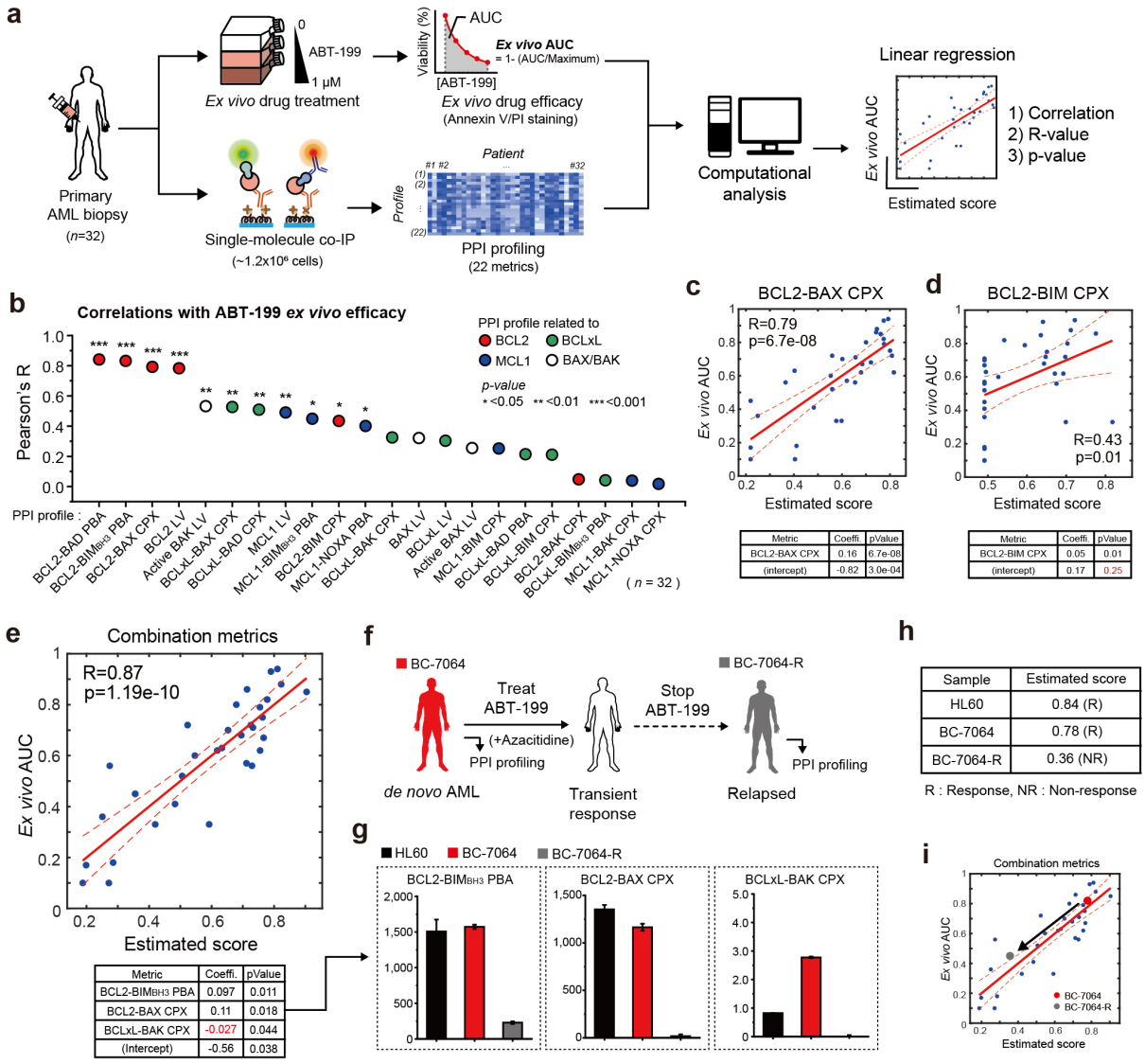

Fig. 4: Constructing an analysis model for ABT-199 efficacy with multi-dimensional PPI profiling. a, Schematic for generating linear regression correlation between *ex vivo* efficacy of ABT-199 and PPI profiles from primary AML samples. The collected AML cells were cultured and treated with 0-1 μM of ABT-199, and the area under curves (AUCs) of cell viability were obtained as *ex vivo* drug efficacy (upper). ~1.2x10^6 of primary AML cells on the same cohort were performed single-molecule co-IP profiling (lower) (*n*=32). **b**, Pearson's correlations

949 between *ex vivo* AUC of ABT-199 and PPI profiles for primary AML biopsies. **c, d**, Correlations
950 between *ex vivo* AUC and single BCL2-related PPI metrics. (c) BCL2-BAX complex, (d) BCL2-
951 BIM complex. **e,** Correlation between *ex vivo* AUC and combination of multiple PPI metrics
952 (BCL2-BIM_{BH3} PBA, BCL2-BAX CPX, and BCLxL-BAK CPX). The statistical indicators
953 (coefficient, *p*-value) of each metric were displayed. **f,** Clinical features and the ABT-199
954 administration history of BC-7064. **g,** Comparison of the PPI profiles from the initial and the
955 relapsed BC-7064 samples. **h,** The estimated scores of BC-7064 and BC-7064-R from model (e).
956 **i,** Investigating the change of the estimated score and *ex vivo* AUC depending on the relapse of
957 the BC-7064.

958

959

960

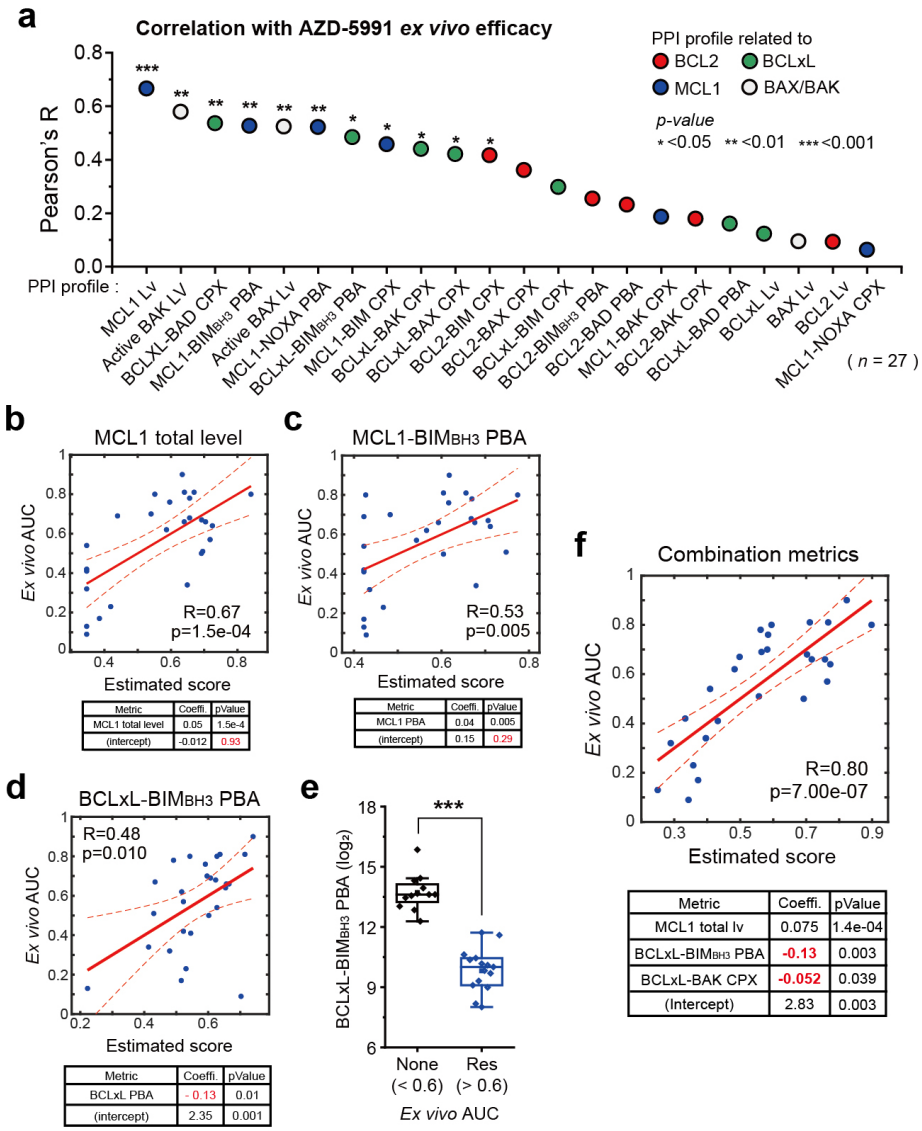

Metric	Coeffi.	pValue
MCL1 total level	0.05	1.5e-4
(intercept)	-0.012	0.93

Metric	Coeffi.	pValue
MCL1 PBA	0.04	0.005
(intercept)	0.15	0.29

Metric	Coeffi.	pValue
BCLxL PBA	- 0.13	0.01
(intercept)	2.35	0.001

Metric	Coeffi.	pValue
MCL1 total lv	0.075	1.4e-04
BCLxL-BIMBH3 PBA	-0.13	0.003
BCLxL-BAK CPX	-0.052	0.039
(Intercept)	2.83	0.003

Fig. 5: Construction of an MCL1 inhibitor efficacy model. a, Pearson's correlations between *ex vivo* AUC of AZD-5991 and PPI profiles for primary AML samples (*n*=27). **b-c**, Correlations between *ex vivo* AUC and single PPI metrics. (b) MCL1 total level, (c) MCL1-BIM_{BH3} PBA. **d**, Negative correlation between *ex vivo* AUC for AZD-5991 and BCLxL-BIM_{BH3} PBA. **e,** Comparison of BCLxL-BIM_{BH3} PBA counts for the AZD-5991 responsive (*ex vivo* AUC > 0.6, *n*=12) and non-responsive (*ex vivo* AUC < 0.6, *n* =15) AML samples (Two-sided two-sample *t*-

968 test, mean difference: 3.90, P=9.09x10^{-11}). **f,** Correlation between *ex vivo* AUC and combination

969 of multiple PPI metrics (MCL1 total level, BCLxL-BIM_{BH3} PBA, BCLxL-BAK CPX). The

970 statistical indicators (coefficient. p-value) of each metric were displayed.

971

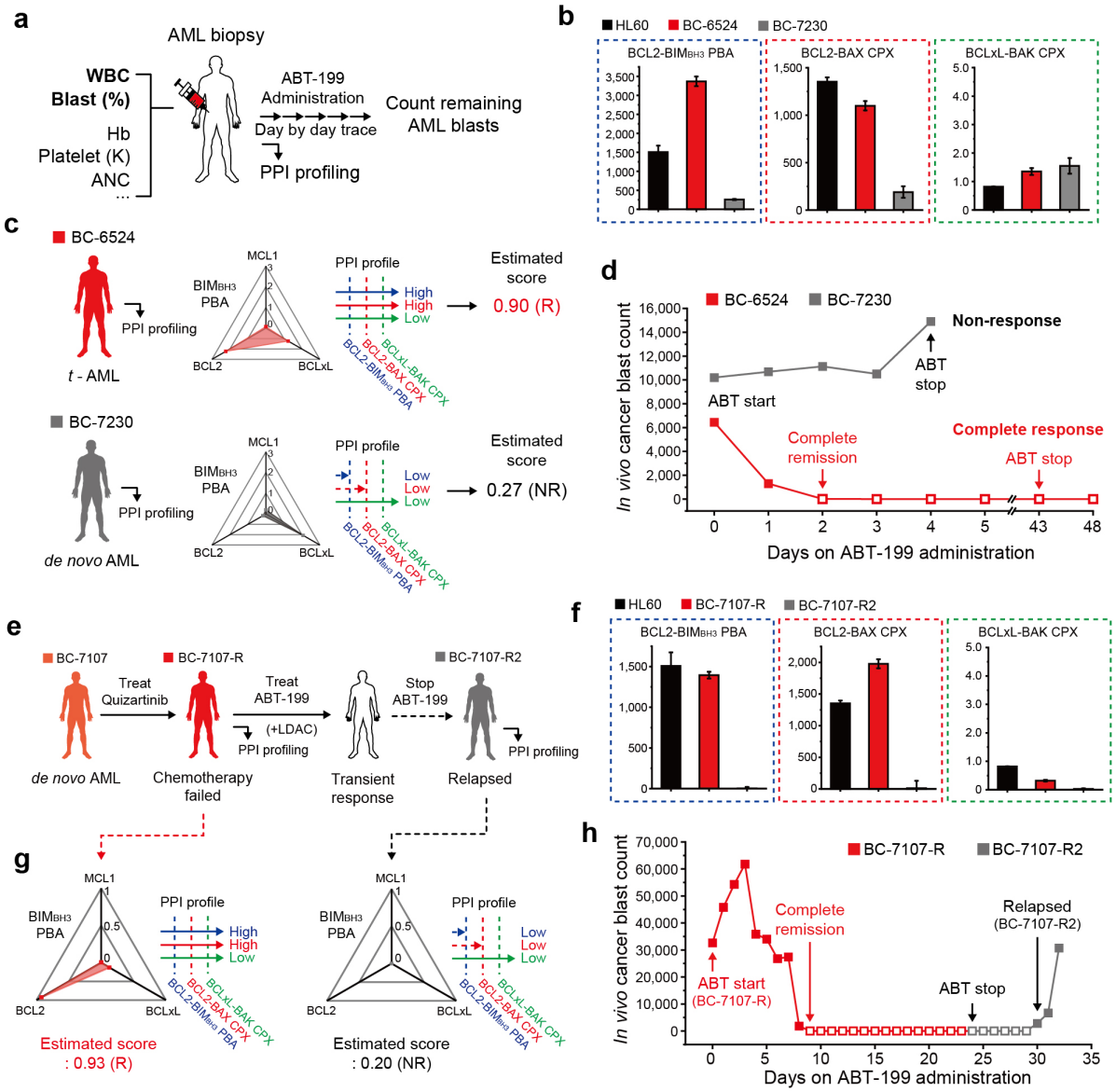

Fig. 6: Using the PPI analysis model as a predictive biomarker for ABT-199 efficacy. a, Complete blood cell count (CBC) analysis for counting the number of cancer blasts in the AML samples. **b-d,** Comparison of the PPI profiles from the BC-6524 and BC-7230 samples. (b) Comparison of PPI profiles for combinatory metrics model, (c) Clinical features and PPI diagnostic results from the BIM_{BH3} PBA profile and ABT-199 efficacy prediction model, (d) Changes of *in vivo* cancer blast counts through the days after ABT-199 administration. **e,** Clinical

979 features and the ABT-199 administration history of BC-7107. **f,** Tracking the changes of PPI
980 profiles after relapse of BC-7107-R. **g,** Tracking the changes of BIM_{BH3}-PBA profiles and PPI
981 diagnostic results after relapse of BC-7107-R. **h,** Changes of *in vivo* cancer blast counts from
982 BC-7107-R through the days after ABT-199 administration. (c, g) The scores were estimated
983 from the model in Figure 4e.